Chapter 14

Extra Dimensions and New Vector Boson High Mass States

14.1 Introduction

The theoretical and phenomenological landscape of beyond the standard model searches extends to a multitude of exotic tendencies today in collider physics. Most are conceived within one kind or another of extra dimensions and supersymmetric scenarios. The strict or loose dualities between different frameworks for physics "beyond the standard model" have a direct experimental consequence: the final states and signatures of the models are very similar. This renders the characterisation of an excess or a deviation a fine and probably long challenge. To mention a couple of examples: the question "is it extra dimensions (*e.g.* UED/ TeV) or is it SUSY?" or "is it a Randall-Sundrum graviton mode or a Z′" is not going to be answered immediately when the excess is observed. The results from all the collider data to date, together with the as yet unobserved Higgs and including the data on the neutrino masses and the composition of the universe, impose a wide program of searches that the LHC experiments are preparing for.

In the present chapter and as well as the "alternatives" chapter that follows, a series of searches is presented with signatures (corresponding to models) as indicated below:

- Dilepton, dijet, diphoton resonances
  - using $ee,\ \mu\mu, \gamma\gamma$, dijets
  - searching for Z' (leptons,jets), RS Extra Dimensions (leptons,photons,jets), Z_{KK} in TeV $^{-1}$ (electrons) (can also be interpreted in the context of Little Higgs models)
- Dilepton, dijet continuum modification
  - using $\mu\mu$, dijets
  - searching for ADD graviton exchange (dimuons), contact interactions (dimuons, dijets)
- Dilepton+dijets
  - using $ee,\ \mu\mu$+dijets
  - searching for heavy neutrino from right-handed W (can also be interpreted in the context of leptoquark searches)
- Single photon+missing E_T
  - using $\gamma + \text{missing } \mathrm{E_T}$
  - searching for ADD direct graviton emission (can also be interpreted in

the context of GMSB gravitino-type searches)

- Single lepton+missing E_T
  - using $\mu + \text{missing } \mathrm{E_T}$
  - searching for W' (can also be interpreted in the context of little Higgs or W_{KK} excitation in TeV $^{-1}$ models)
- Multilepton+multijet
  - using top, W and Z reconstruction and constraints
  - searching for technicolour, littlest Higgs (can also be interpreted in the context of leptoquark searches)
- Same-sign dileptons
  - using $ee, \mu\mu, e\mu$
  - searching for same-sign top (can be interpreted in the context of technicolour, charged Higgs or SUSY searches)
- High multiplicity/sphericity
  - searching for microscopic black holes in large extra dimensions scenarios

Although not included here, a number of searches are being developed for signatures that involve heavy highly-ionising charged particles and split-SUSY type R-hadrons as well as low P_T multi-lepton signatures in UED scenarios. Strategies are being developed to extract the Standard Model backgrounds from data and control its systematic uncertainties. Fake rates are being estimated as possible while machine and cosmic ray induced backgrounds are not included although methods to suppress them are being developed.

14.1.1 Models with heavy vector bosons

Additional heavy neutral gauge bosons (Z′) are predicted in many superstring-inspired [86, 87] and grand unified theories (GUTs) [88], as well as in dynamical symmetry breaking [89] and "little Higgs" [90] models. There are no reliable theoretical predictions, however, of the Z′ mass scale. Current lower limits on the Z′ mass are (depending on the model) of the order of 600–900 GeV/c^2 [54]. The mass region up to about 1 TeV/c^2 is expected to be explored at Run II at the Tevatron [91, 92]. The LHC offers the opportunity to search for Z′ bosons in a mass range significantly larger than 1 TeV/c^2. In the Z′ studies presented here (sections 14.3 and 14.2) six models which are frequently discussed and whose properties are representative of a broad class of extra gauge bosons are used:

- $\mathrm{Z_{SSM}}$ within the Sequential Standard Model (SSM), which has the same couplings as the Standard Model Z^0
- Z_ψ, Z_η and Z_χ, arising in $\mathrm{E_6}$ and SO(10) GUT groups with couplings to quarks and leptons as derived in Refs. [95, 96].
- $\mathrm{Z_{LRM}}$ and $\mathrm{Z_{ALRM}}$, arising in the framework of the so-called "left-right" [97] and "alternative left-right" [91, 92] models with couplings as derived in Ref. [91, 92], with the choice of $g_R = g_L$.

The W' search presented in section 14.4 uses a reference model by Altarelli [697], in which the W' is a heavy copy of the W, with the very same left-handed fermionic couplings (including CKM matrix elements), while there is no interaction with the Standard Model gauge bosons or with other heavy gauge bosons such as a Z'.

14.1.2 Arkani-Hamed Dimopoulos Dvali (ADD) models

ADD refers to the class of models which incorporate the large extra dimensions scenario of Arkani-Hamed, Dvali, and Dimopoulos [698]. These were the first extra dimensions models in which the compactified dimensions can be of macroscopic size, consistent with all current measurements, and they are referred to as "large extra dimensions" models. In the most basic version, n extra spatial dimensions are compactified on a torus with common circumference R, and a brane is introduced which extends only in the three infinite spatial directions. Strictly speaking, the brane should have a very small tension (energy per unit volume) in order that it does not significantly warp the extra dimensional space. It is assumed that all standard model fields extend only in the brane. This can be considered as a toy version of what happens in string theory, where chiral gauge theories similar to the standard model are confined to reasonably simple brane configurations in reasonably simple string compactifications [699].

A consequence of these assumptions is that the effective 4d Planck scale is related to the underlying fundamental Planck scale of the $4+n$-dimensional theory and to the volume of the compactified space. This relation follows from Gauss' Law, or by dimensional analysis

$$M_{\rm Planck}^2 = M_*^{2+n}\, R^n \quad , \tag{14.1}$$

where $M_{\rm Planck}^2$ is defined by Newton's constant: $M_{\rm Planck} = 1/\sqrt{G_N} = 1.2 \times 10^{19}\,{\rm GeV/c^2}$. M_*^{2+n} is defined as the gravitational coupling which appears in the $4+n$-dimensional version of the Einstein-Hilbert action. It is the quantum gravity scale of the higher dimensional theory.

If $M_{\rm Planck}$, M_* and $1/R$ are all of the same order, as is usually assumed in string theory, this relation is not very interesting. But it is plausible and experimentally allowed that M_* is equal to some completely different scale. Taking $M_* \sim 1\,{\rm TeV/c^2}$ [700] the hierarchy problem of the standard model is translated from an ultraviolet problem to an infrared one. Note that if there is any interface with string theory, ADD-like models must arise from string ground states in which the string scale (and thus the ultraviolet cutoff for gravity) is also in the TeV range. This is difficult to achieve but has been studied in [701].

The ADD scenario renders observations of quantum gravity at the LHC possible. In such models only the graviton, and possibly some non-SM exotics like the right-handed neutrino, probe the full bulk space. There is a Kaluza-Klein tower of graviton modes, where the massless mode is the standard 4d graviton, and the other KK modes are massive spin 2 particles which also couple to SM matter with gravitational strength.

Whereas bremsstrahlung of ordinary gravitons is a completely negligible effect at colliders, the total cross section to produce *some* massive KK graviton is volume enhanced, and effectively suppressed only by powers of M_* and not $M_{\rm Planck}$. From Eq. (14.1) it follows :

$$\sigma \sim \frac{1}{M_{\rm Planck}^2}(ER)^n \sim \frac{1}{M_*^2}(EM_*)^n \quad , \tag{14.2}$$

where E is the characteristic energy of the subprocess.

For graviton phenomenology it is useful to replace the ADD parameter M_* by other rescaled parameters. The two most useful choices are taken from the work of Giudice, Rattazzi and

Wells (GRZ) [702], and Han, Lykken and Zhang (HLZ) [703]:

$$M_*^{n+2} = \frac{S_{n-1}}{(2\pi)^n} M_s^{n+2} \,, \tag{14.3}$$

$$M_*^{n+2} = \frac{8\pi}{(2\pi)^n} M_D^{n+2} \,, \tag{14.4}$$

where M_s is the HLZ scale, M_D is the GRW scale, and S_{n-1} is the surface area of a unit n-sphere:

$$S_{n-1} = \frac{2\pi^{n/2}}{\Gamma(n/2)} \,. \tag{14.5}$$

Both notations are equivalent. To obtain a complete dictionary between ADD, GRZ and HLZ, one also needs to relate the ADD parameter R to those used by the other authors: $R = R_{\rm HLZ} = 2\pi R_{GRW}$, and take note of the different notations for Newton's constant:

$$\kappa^2 = 16\pi G_N \text{ (HLZ)}; \quad \bar{\rm M}_{\rm P}^2 = \frac{1}{8\pi {\rm G_N}} \text{ (GRW)} \,. \tag{14.6}$$

A Kaluza-Klein (KK) graviton mode has a mass specified by an n-vector of integers $\vec{k}$:

$$m^2(\vec{k}) = \frac{\vec{k}^2}{R_{\rm GRW}^2} \,. \tag{14.7}$$

Let $r = |\vec{k}|$. Then for large r (as is often the relevant case for ADD phenomenology) the number of KK graviton states of a given polarisation with $r \le r_{\rm max}$ is given by the integral

$$\begin{aligned} S_{n-1} \int_0^{r_{\rm max}} dr\, r^{n-1} &= \frac{1}{n} S_{n-1}\, r_{\rm max}^n \\ &= \int_0^{m_{\rm max}} \rho(m)\, dm \,, \end{aligned} \tag{14.8}$$

where the KK density of states is

$$\rho(m) = \frac{m^{n-1}}{G_N M_s^{n+2}} \,. \tag{14.9}$$

M_s is the natural scaling parameter for KK graviton production. The density of states formulation can be applied to a much more general class of models than ADD, and can also include graviton wavefunction factors when the extra dimensions are not flat.

Consider an on-shell production of a KK graviton from a pp or collision. To leading order this is a $2 \to 2$ process with two massless partons in the initial state, plus a massive KK graviton and a massless parton in the final state. Let p_1, p_2 denote the 4-momenta of the initial state partons, p_3 the 4-momentum of the graviton, and p_4 the 4-momentum of the outgoing parton. The total cross section for any particular variety of partonic subprocess has the form

$$\sigma(1+2 \to {\rm KK}+4) = \int dx_1 dx_2\, f_1(x_1,\hat{s}) f_2(x_2,\hat{s}) \int d\hat{t} \int_0^{\sqrt{\hat{s}}} dm\, \rho(m)\, \frac{d\sigma_m}{d\hat{t}}(\hat{s},\hat{t}) \,, \tag{14.10}$$

where $f_1(x_1,\hat{s})$, $f_2(x_2,\hat{s})$ are the parton distribution functions (pdfs) for the initial state partons, $\hat{s} = x_1 x_2 s = (p_1+p_2)^2$ is the square of the total centre of mass (cm) energy of the subprocess, and $\hat{t} = (p_1 - p_3)^2$ is the usual Mandelstam invariant. The formulae for $d\sigma_m/d\hat{t}$, the differential subprocess cross sections for KK gravitons of mass m, are given in [702].

14.1.2.1 Graviton production above the cutoff

At the LHC, proton–proton collisions will probe a distribution of partonic subprocess energies $\sqrt{\hat{s}}$. This creates a problem for the consistent analysis of missing energy signatures in the framework of ADD models. These models are simple low energy effective theories which are only valid for $\sqrt{\hat{s}}$ below some cutoff. This cutoff is at most $2M_*$, and could be a factor of a few smaller if the ultraviolet completion of the model is weakly coupled string theory [704]. The same is true for the Lykken–Randall model [705], which is a low energy description of gravity in a single infinite warped extra dimension, valid up to a cutoff $\sim M_*$. It is inconsistent to use either type of model to describe LHC collisions with subprocess energies greater than the cutoff.

This problem was first noted by the authors of [702], who suggested replacing the ADD graviton density of states $\rho(m)$ by $\rho(m)\theta(\sqrt{\hat{s}} - M_D)$, where θ is a step function. This introduces a systematic theory error into the analysis. The size of this error is very sensitive to the values of M_D and n. For initial LHC data sets, we will be probing the lower range of M_D values, beginning at the current $\simeq 1\,\text{TeV/c}^2$ bounds from Tevatron and LEP. This increases the theory systematic from the cutoff for any fixed n. For fixed M_D, the theory systematic increases rapidly for increasing n. For $n = 2$, the theory uncertainty in the total cross section remains below about 20% even for M_D approaching $1\,\text{TeV/c}^2$.* For $n = 6$ and above, the effect of the cutoff is enormous for modest values of M_D, because the rapid rise in the graviton density of states is not compensated by the rapid falloff of the pdfs. The theory error for the total cross section in this case can be as large as an order of magnitude.

The resolution of this problem depends upon whether or not there is a signal in the missing energy channels (we will not discuss the related problems which arise in channels affected by virtual graviton exchanges). If there is a signal, the optimal procedure is to measure the observables $d^2\sigma/dp_T d\eta$ as accurately as possible, perhaps at more than one collider energy as suggested in [706, 707]. No theory systematic should be included in these analyses. Instead, one should use the data to find the best fit form for $\rho(m, \sqrt{\hat{s}})$. Simple trial forms can be obtained, for example, from multiplying the ADD density of states by the form factors obtained in models with strings [704, 708, 709] or branes [710]. For the lower range of M_D values, the sensitivity to n suggested in [706, 707] will tend to be washed out. This is not a bad outcome, since it is a result of convolving the n dependence with the effects of strings, branes or other new physics. Thus the theory systematic is replaced by likelihood fits to theories of Planck scale physics.

More problematic is the case where there is no graviton signal in a given data set. Since in this case we are trying to set a limit, we need an estimate of the theory systematic. The simplest possibility is to implement the GRW cutoff defined above, and estimate the theory error by varying the cutoff. For ADD with $n \geq 6$, one expects to obtain no lower bound at all on M_D, as noted in [702].

14.1.3 Virtual graviton exchange

The second class of collider signals for large extra dimensions is that of virtual graviton exchange[702, 711] in $2 \to 2$ scattering. This leads to deviations in cross sections and asymmetries in Standard Model processes with difermion final states. It may also give rise to new production processes which are not present at tree-level in the Standard Model, such as

*To avoid strong astrophysical constraints, $n = 2$ ADD models also require an *ad hoc* infrared cutoff, truncating the massive graviton spectrum for masses below about 20 MeV. This has a negligible effect on LHC analysis.

$gg \to \ell^+\ell^-$. The signature is similar to that expected in composite theories and provides a good experimental tool for searching for large extra dimensions for the case $\sqrt{s} < M_D$.

Graviton exchange is governed by the effective Lagrangian

$$\mathcal{L} = i\frac{4\lambda}{M_H^4} T_{\mu\nu} T^{\mu\nu} + h.c. \tag{14.11}$$

The amplitude is proportional to the sum over the propagators for the graviton KK tower which may be converted to an integral over the density of KK states. However, in this case, there is no specific cut-off associated with the process kinematics and the integral is divergent for $n > 1$. This introduces a sensitivity to the unknown ultraviolet physics which appears at the fundamental scale. This integral needs to be regulated and several approaches have been proposed: (i) a naive cut-off scheme [702, 711] (ii) brane fluctuations [710], or (iii) the inclusion of full weakly coupled TeV-scale string theory in the scattering process [704, 708]. The most model independent approach which does not make any assumptions as to the nature of the new physics appearing at the fundamental scale is that of the naive cut-off. Here, the cut-off is set to $M_H \neq M_D$; the exact relationship between M_H and M_D is not calculable without knowledge of the full theory. The parameter $\lambda = \pm 1$ is also usually incorporated in direct analogy with the standard parametrisation for contact interactions [122] and accounts for uncertainties associated with the ultraviolet physics. The substitution

$$\mathcal{M} \sim \frac{i^2\pi}{M_{\rm Pl}^2} \sum_{\vec{n}=1}^{\infty} \frac{1}{s - m_{\vec{n}}^2} \to \frac{\lambda}{M_H^4} \tag{14.12}$$

is then performed in the matrix element for s-channel KK graviton exchange with corresponding replacements for t- and u-channel scattering. As above, the Planck scale suppression is removed and superseded by powers of $M_H \sim$ TeV/c^2.

The resulting angular distributions for fermion pair production are quartic in $\cos\theta$ and thus provide a unique signal for spin-2 exchange.

The experimental analyses also make use of the cut-off approach. Using virtual Kaluza-Klein graviton exchange in reactions with diphoton, dibosons and dilepton final states, ($G_n \to \gamma\gamma, VV, \ell\ell$), the LEP and Tevatron experiments exclude exchange scales up to ~ 1.1 TeV/c^2.

In the dimuon studies presented here (14.3.2) with 1 fb^{-1} a 5-sigma effect from the virtual contributions of ADD gravitons to Drell-Yan process is observable for effective fundamental Planck scale of 4.0 TeV and for $n = 6$ extra dimensions.

14.1.4 Inverse TeV sized extra dimensions

The possibility of TeV $^{-1}$-sized extra dimensions naturally arises in braneworld theories [700]. By themselves, they do not allow for a reformulation of the hierarchy problem, but they may be incorporated into a larger structure in which this problem is solved. In these scenarios, the Standard Model fields are phenomenologically allowed to propagate in the bulk. This presents a wide variety of choices for model building: (i) all, or only some, of the Standard Model gauge fields exist in the bulk; (ii) the Higgs field may lie on the brane or in the bulk; (iii) the Standard Model fermions may be confined to the brane or to specific locales in the extra dimension. The phenomenological consequences of this scenario strongly depend on the location of the fermion fields. Unless otherwise noted, our discussion assumes that all of the Standard Model gauge fields propagate in the bulk.

The masses of the excitation states in the gauge boson KK towers depend on where the Higgs boson is located. If the Higgs field propagates in the bulk, the zero-mode state of the Higgs KK tower receives a vacuum expectation value (vev) which is responsible for the spontaneous breaking of the electroweak gauge symmetry. In this case, the resulting mass matrix for the states in the gauge boson KK towers is diagonal and the excitation masses are shifted by the mass of the gauge zero-mode, which corresponds to the Standard Model gauge field, giving

$$m_{\vec{n}} = (m_0^2 + \vec{n} \cdot \vec{n}/R_c^2)^{1/2} \tag{14.13}$$

where $\vec{n} = (n_1, n_2, ...)$ labels the KK excitation levels. However, if the Higgs is confined to the brane, its vev induces mixing, amongst the gauge KK states of order $(m_0 R_c)^2$. The KK mass matrix must then be diagonalised in order to determine the excitation masses. For the case of 1 extra TeV $^{-1}$-sized dimension, the coupling strength of the gauge KK states to the Standard Model fermions on the brane is $\sqrt{2}g$, where g is the corresponding Standard Model gauge coupling.

In the case where the Standard Model fermions are rigidly fixed to the brane they do not feel the effects of the additional dimensions. For models in this class, precision electroweak data place strong constraints on the mass of the first gauge KK excitation. Contributions to electroweak observables arise from the virtual exchange of gauge KK states and a summation over the contributions from the entire KK tower must be performed. For $D > 5$, this sum is divergent. In the full higher dimensional theory, some new, as of yet unknown, physics would regularise this sum and render it finite. An example of this is given by the possibility that the brane is flexible or non-rigid, which has the effect of exponentially damping the sum over KK states. Due to our present lack of knowledge of the full underlying theory, the KK sum is usually terminated by an explicit cut-off, which provides a naive estimate of the magnitude of the effects.

Since the $D = 5$ theory is finite, it is the scenario that is most often discussed and is sometimes referred to as the 5-dimensional Standard Model (5DSM). In this case, a global fit to the precision electroweak data including the contributions from KK gauge interactions yields $m_1 \sim R_c^{-1} \gtrsim 4\,\text{TeV/c}^2$. In addition, the KK contributions to the precision observables allow for the mass of the Higgs boson to be somewhat heavier than the value obtained in the Standard Model global fit. Given the constraint on R_c from the precision data set, the gauge KK contributions to the anomalous magnetic moment of the muon are small. The first gauge KK state can be produced as a resonance at the LHC in the Drell-Yan channel provided $m_1 \lesssim 6\,\text{TeV/c}^2$. In the studies presented here using the Z_{KK} in the dielectron channel a 5-sigma reach for $m_1 \sim R_c^{-1} \sim 4.97\,\text{TeV/c}^2$ is obtained with $10\,\text{fb}^{-1}$.

In the scenario where the Standard Model fermions are localised at specific points in the extra TeV $^{-1}$-sized dimensions, the fermions have narrow gaussian-like wave functions in the extra dimensions with width much smaller than R_c^{-1}. The placement of the different fermions at distinct locations in the additional dimensions, along with the narrowness of their wavefunctions, can then naturally suppress operators mediating dangerous processes such as proton decay. The exchange of gauge KK states in $2 \to 2$ scattering processes involving initial and final state fermions is sensitive to the placement of the fermions and can be used to perform a cartography of the localised fermions, *i.e.* , measure the wavefunctions and locations of the fermions. At very large energies, it is possible that the cross section for such scattering will tend rapidly to zero since the fermions' wavefunctions will not overlap and hence they may completely miss each other in the extra dimensions.

14.1.5 Randall-Sundrum (RS) models

Randall-Sundrum refers to a class of scenarios, also known as warped extra dimensions models, originated by Lisa Randall and Raman Sundrum [93, 646]. In these scenarios there is one extra spatial dimension, and the five-dimensional geometry is "warped" by the presence of one or more branes. The branes extend infinitely in the usual three spatial dimensions, but are sufficiently thin in the warped direction that their profiles are well-approximated by delta functions in the energy regime of interest. If we ignore fluctuations of the branes, we can always choose a "Gaussian Normal" coordinate system, such that the fifth dimension is labelled y and the usual 4d spacetime by x^μ. The action for such a theory contains, at a minimum, a 5d bulk gravity piece and 4d brane pieces. The bulk piece has the 5d Einstein-Hilbert action with gravitational coupling M^3, and a 5d cosmological constant Λ. The brane pieces are proportional to the brane tensions V_i, which may be positive or negative. These act as sources for 5d gravity, contributing to the 5d stress-energy terms proportional to

$$\sum_i V_i \delta(y - y_i) \tag{14.14}$$

where the y_i are the positions of the branes. Combined with a negative Λ, this results in a curved geometry, with a 5d metric of the form:

$$\begin{aligned} g_{\mu\nu}(x^\rho, y) &= a^2(y)\, \tilde{g}_{\mu\nu}(x^\rho) \ , \\ g_{\mu y} = 0 \ , &\quad g_{yy} = 1 \ , \end{aligned} \tag{14.15}$$

where $a(y)$ is called the warp factor, $\tilde{g}$ is a 4d metric, and I have made a useful choice of coordinates. Warping refers to the fact that a 4d distance d_0 measured at $y = y_0$ is related to an analogous 4d distance d_1 measured at $y = y_1$ by $a(y_0)d_0 = a(y_1)d_1$. Thus in Randall-Sundrum scenarios 4d length, time, energy and mass scales vary with y.

Most collider physics phenomenology done with warped extra dimensions so far is based upon one very specific model, the original simple scenario called RSI. In this model the extra dimension is compactified to a circle of circumference $2L$, and then further orbifolded by identifying points related by $y \to -y$. The fifth dimension then consists of two periodically identified mirror copies of a curved 5d space extending from $y = 0$ to $y = L$. It is assumed that there is a brane at $y = 0$, with positive tension V_0; it is known as the Planck brane - strong gravity resides on that brane. There is another brane at $y = L$, with negative tension V_L, known as the TeV brane - the entire 4d universe is confined to the TeV brane.

Randall and Sundrum showed that, for a tuned choice of input parameters $V_0 = -V_L = -M^2\Lambda$, the 5d Einstein equations have a simple warped solution on $0 < y < L$ with metric:

$$\begin{aligned} g_{\mu\nu}(x^\rho, y) &= \mathrm{e}^{-2ky}\, \eta_{\mu\nu} \ , \\ g_{\mu y} = 0 \ , &\quad g_{yy} = 1 \ , \end{aligned} \tag{14.16}$$

where $\eta_{\mu\nu}$ is the 4d flat Minkowski metric, and $k = \sqrt{-\Lambda}$. Away from the branes, the 5d curvature is constant and negative; it is thus equivalent locally to AdS_5, with the Anti-de Sitter radius of curvature given by $1/k$. At the locations of the branes the curvature is discontinuous, due to the fact that the branes are delta function sources for curvature.

The RSI model is completely described by three parameters: k, M, and L. Restricting the scenario to a low energy effective description implies considering $k, 1/L \ll M$. In fact in RSI it is assumed that k is merely parametrically small compared to the 5d Planck scale M, i.e.

$k \sim M/10$. The effective 4d Planck scale, which is the same as the coupling of the graviton zero mode, is given by dimensional truncation:

$$M^2_{\text{Planck}} = \frac{M^3}{2k}\left(1 - \mathrm{e}^{-2kL}\right) \ . \tag{14.17}$$

Then, within an order of magnitude, $M \sim k \sim M_{\text{Planck}}$. In RSI the distance L is fixed by requiring that $a(L)M_{\text{Planck}} \simeq 1\,\text{TeV}$, thus $kL \sim 30$. This is *not* a large extra dimension: its inverse size is comparable to the grand unification scale.

Since the standard model fields live on the TeV brane as in ADD models, the phenomenology of RSI is concerned with the effects of the massive KK modes of the graviton. These modes as measured on the TeV brane have their mass splittings of the order of a TeV, and have TeV suppressed couplings to the standard model fields. In RSI, the Standard Model is replaced at the TeV scale by a new effective theory in which gravity is still very weak, but there are exotic heavy spin-two particles.

At the LHC the KK gravitons of RSI would be seen as difermion or dibosons resonances, since (unlike the KK gravitons of ADD) the coupling of each KK mode is only TeV suppressed [712]. The width of these resonances is controlled by the ratio $c = k/M$; the resonances become more narrow as the coupling parameter $c = k/M$ is reduced, as shown in Figure 14.1.

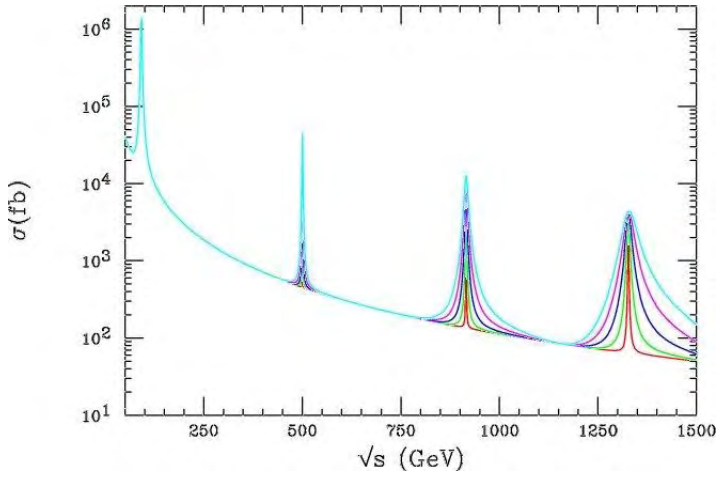

Figure 14.1: The cross section for $e^+e^- \to \mu^+\mu^-$ including the exchange of KK gravitons in the RSI model. The narrowest resonances correspond to $k/M = 0.05$, the widest to $k/M = 0.14$. (taken from reference [713]).

The studies presented here focus on dilepton and diphoton final states while results using dijets can be found in section 4.1. Note that due to the spin-2 nature of the graviton its branching ratio to diphotons is roughly twice that of a single dilepton channel.

14.2 High mass dielectron final states

This section presents the CMS experiment discovery potential for new heavy resonances, decaying into an electron pair. The $\mathrm{e}^+\mathrm{e}^-$ decay channel provides a clean signature in the CMS detector. The presence of a heavy particle would be detected in CMS by the observation

of a resonance peak in the dielectron mass spectrum over the Drell-Yan process ($\mathrm{pp} \rightarrow \gamma/\mathrm{Z} \rightarrow \mathrm{e}^{+}\mathrm{e}^{-}$) which constitutes the main Standard Model background.

Heavy resonances with mass above 1 TeV/c^2 are predicted by several models beyond the Standard Model. Three models are considered here: Kaluza-Klein (KK) excitations of a Z boson (TeV $^{-1}$ model, see Section 14.1.4) and KK excitation of a graviton (Randall-Sundrum (RS) model, see Section 14.1.5), both predicted in extra dimensions models, and neutral heavy Z' boson predicted by Grand Unified Theories (GUT) (see Section 14.1.1). For the Z' bosons, 6 models are studied, as for the $Z' \rightarrow \mu^{+}\mu^{-}$ channel [99] that is discussed in Section 14.3.

Details of the analyses presented in this section can be found in [714] and [715].

14.2.1 Event selection and correction

Two electrons are required for this analysis. They are reconstructed as super-clusters (SC) in the ECAL calorimeter in the barrel and the endcap regions [716]. For endcap SC, the energy loss in the preshower detector is taken into account. The two SC with highest energies are selected as the electron candidates.

Reducible backgrounds (like QCD jets and γ-jets) are suppressed by applying the following requirements:

- The ratio of the HCAL to ECAL energy deposits is required to be $H/E < 10$ %.
- The two SC must be isolated: the total additional transverse energy in a cone of radius $0.1 < \Delta R < 0.5$ is required to be below 2 % of the SC transverse energy (where $\Delta R = \sqrt{\Delta\eta^2 + \Delta\phi^2}$).
- To identify electrons and reject neutral particles, a track is requested to be associated for each electron candidate. If a track is associated with only one of these SC, the event is however kept if it contains a third SC with $E > 300\,\mathrm{GeV}$ with an associated track and satisfying the H/E and isolation cuts described above.

The selected events are then corrected for the following effects:

- Saturation correction: For very energetic electrons and photons, saturation occurs in the ECAL electronics because of the limited dynamical range of the Multi-Gain-Pre-Amplifier. The saturation threshold has been established to be at 1.7 TeV in crystals of the barrel and 3.0 TeV in the endcaps. A correction method (for barrel only) has been developed using the energy deposit in crystals surrounding the saturated crystal. The correction allows the energy deposits of clusters suffering from saturation to be estimated with a resolution of about 7% [717].
- Energy correction: The ECAL measured electron energy after preshower, HCAL and saturation corrections, is smaller than the generated energy. Dedicated energy correction factors for very energetic electrons have been determined using calibration files. These factors depend on both energy, η and whether saturation occurs or not. The resolution on the corrected SC energy is 0.6 % at $E = 1000\,\mathrm{GeV}$.
- z-vertex distribution: The measurement in η takes into account the knowledge of the z-vertex position.
- FSR recovery: Hard photon emission from Final State Radiation can induce the detection in the event of a third energetic SC If a SC with $E > 300\,\mathrm{GeV}$ satisfying the H/E and isolation cuts is observed very close to the SC of the electron candi-

dates ($\Delta R < 0.1$), this additional SC is associated to the corresponding electron.

14.2.2 Mass peak distributions

The resonance mass is reconstructed from the energies and angles of the 2 electron candidates, after the selection cuts and energy corrections mentioned above. Figures 14.2(a) and (b) show the ratio of the reconstructed and the true masses, $M_{\rm ee}/M_{\rm true}$, before and after energy corrections for KK Z production with M =4 and 6 TeV/c^2, respectively. The peaks at low values of $M_{\rm ee}/M_{\rm true}$ correspond to events with saturated ECAL electronics. The final resolution on the resonance mass is around 0.6 % for events with no saturation, and 7 % in case of saturation.

Figure 14.3(a) presents the signal and the Drell-Yan background for KK Z boson production with $M = 4$ TeV/c^2; Figure 14.3(b) for Z' boson production with $M = 1.5$ TeV/c^2; Figure 14.3(c) for graviton production with $M = 1.5$ TeV/c^2 and coupling parameter, defined in Section 14.1.5, $c = 0.01$.

14.2.3 Discovery potential of CMS

The discovery potential of a new physics resonance is determined using the likelihood estimator S_{cL} (defined in Appendix A.1) based on event counting, suited for small event samples. The discovery limit is defined by $S_{cL} > 5$.

The number of signal and background events, $N_{\rm s}$ and $N_{\rm b}$, computed for a given mass window around the peak, are presented in Table 14.1 for he three models, together with the corresponding significance, for an integrated luminosity of 30 fb^{-1}.

The 5 σ discovery limits as a function of mass are given in Fig. 14.4(a) and Fig. 14.4(b), for KK Z boson production and Z' production (for the 6 considered models), respectively. In the graviton case, the 5 σ discovery plane as a function of the coupling parameter c and the resonance mass is given in Fig. 14.4(c).

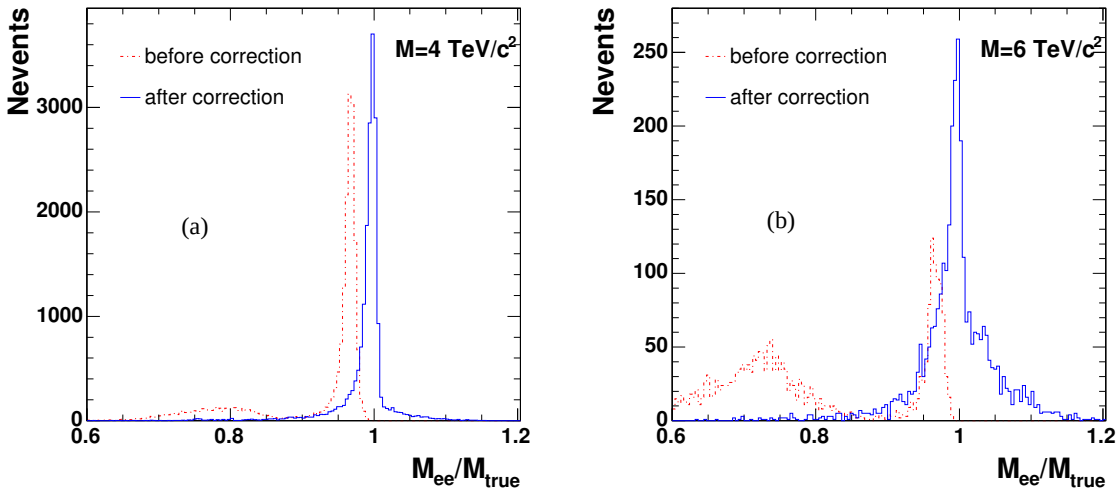

Figure 14.2: Ratio $M_{\rm ee}/M_{\rm true}$ before and after corrections for KK Z boson production, for $M = 4$ TeV/c^2 (a) and $M = 6$ TeV/c^2 (b).

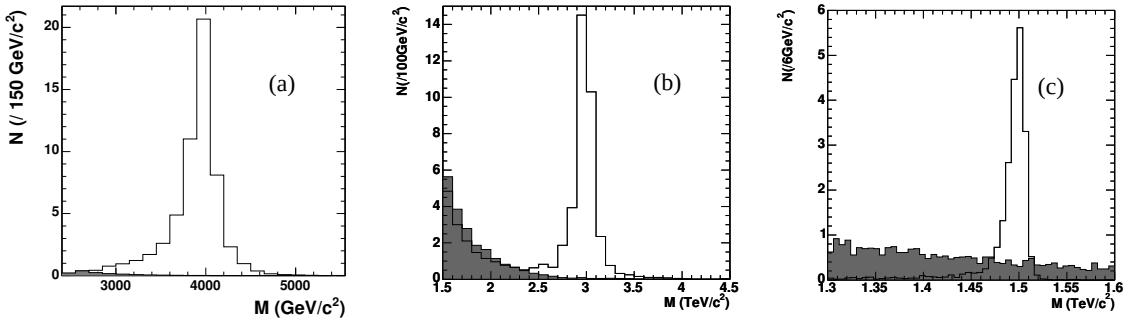

Figure 14.3: Resonance signal (white histograms) and Drell-Yan background (shaded histograms) for KK Z boson production with $M = 4.0\,\text{TeV/c}^2$ (a), SSM Z' boson production with $M = 3.0\,\text{TeV/c}^2$ (b), and graviton production with $M = 1.5\,\text{TeV/c}^2$, coupling parameter $c = 0.01$ (c), for an integrated luminosity of $30\,\text{fb}^{-1}$.

For KK Z bosons, a 5 σ discovery can be achieved for a resonance mass up to $M = 4.97\,\text{TeV/c}^2$ for an integrated luminosity of $10\,\text{fb}^{-1}$, $M = 5.53\,\text{TeV/c}^2$ for $30\,\text{fb}^{-1}$ and $M = 5.88\,\text{TeV/c}^2$ for $60\,\text{fb}^{-1}$. For gravitons, with an integrated luminosity of $30\,\text{fb}^{-1}$, a 5 σ discovery can be extracted for masses up to 1.64 TeV/c^2 for $c = 0.01$ and up to 3.81 TeV/c^2 for $c = 0.1$. For Z' boson production, with an integrated luminosity of $30\,\text{fb}^{-1}$, a 5 σ discovery can be extracted for masses up to 3.31 TeV/c^2 for model ψ and up to 4.27 TeV/c^2 for model ARLM. The 5 σ discovery limits on the resonance masses for 10, 30 and $60\,\text{fb}^{-1}$ are summarised in Table 14.2.

For KK Z boson production, the luminosities needed for a five σ discovery are 1.5, 4.0, 10.8, 29.4, and $81.4\,\text{fb}^{-1}$ for $M = 4.0$, 4.5, 5.0, 5.5 and 6.0 TeV/c^2, respectively; for SSM Z' boson production, they are 0.015, 3.0 and $260\,\text{fb}^{-1}$ for $M = 1$, 3 and 5 TeV/c^2; for graviton production, most of the interesting region of the (mass, coupling) plane is already covered with $10\,\text{fb}^{-1}$.

For KK Z and Z' production, a K factor of 1 was conservatively taken for both the signal and the Drell-Yan background, since heavy Z production interferes with Z/γ Drell-Yan production. For the graviton analysis, as little interference is present with the Standard Model processes, a K factor of 1.0 is used for the signal and of 1.3 for the Drell-Yan background, in order to take into account the higher order terms in the cross section. The latter number comes from the CDF analysis [718] and is compatible with the K factor obtained from theoretical computations [347].

Table 14.1: Number of events for resonant signal, N_s, and for Drell-Yan background, N_b, and corresponding significances S_{cL} for an integrated luminosity of $30\,\text{fb}^{-1}$. The masses M and the mass windows M_w are in TeV/c^2.

	KK Z		G, $c = 0.01$	G, $c = 0.1$	SSM Z'	
M	4.0	6.0	1.5	3.5	1.0	5.0
M_w	3.5-4.5	5.0-6.7	1.47-1.52	3.30-3.65	0.92-1.07	4.18-5.81
N_s	50.6	1.05	18.8	7.30	72020	0.58
N_b	0.13	0.005	4.16	0.121	85.5	0.025
S	22.5	3.0	6.39	6.83	225	1.63

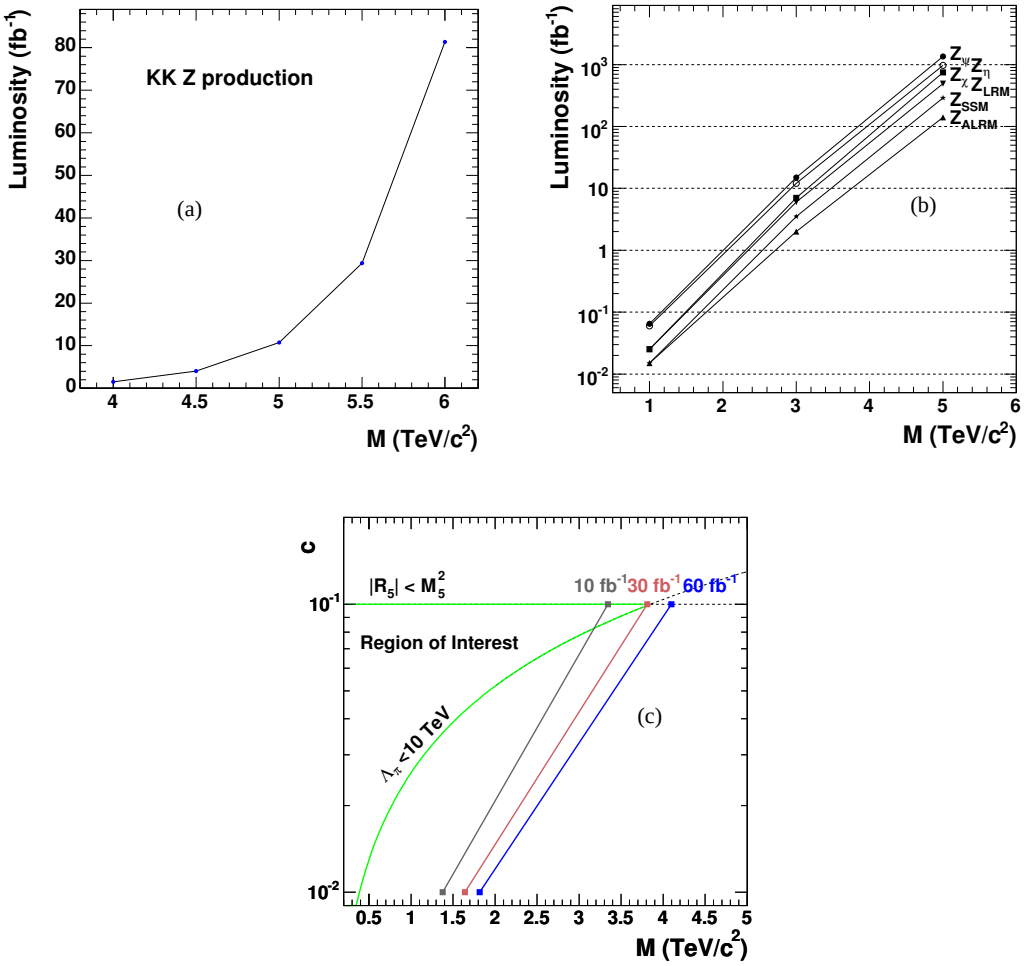

Figure 14.4: Five σ discovery limit as a function of the resonance mass for KK Z boson production (a), for the 6 Z' models (b); five σ discovery plane for graviton production as a function of the coupling parameter c and the graviton mass (c).

14.2.4 Systematic uncertainties

The uncertainty coming from the choice of the parton distribution function (PDF) was investigated using the set of 20 positive and 20 negative errors, of the CETQ6.1M "best fit" parametrisation [12, 719, 720]. For each event, a weight factor is computed according to the x_1, x_2, and Q^2 variables, for each of the 40 PDF errors, in the case of graviton production with $M = 1.5$ TeV/c^2 ($c = 0.01$) and $M = 3.5$ TeV/c^2 ($c = 0.1$). The uncertainties on the PDF modify the number of signal events by a factor 1.20 (positive deviations) and 0.86 (negative deviations) for $M = 1.5$ TeV/c^2 ($c = 0.01$). The corresponding numbers for $M = 3.5$ TeV/c^2 ($c = 0.1$) are 1.47 and 0.78. For the Drell-Yan background, the re-weighting effects on the numbers of events are 1.07 and 0.94 for masses around 1.5 TeV/c^2, and 1.19 and 0.88 for masses around 3.5 TeV/c^2. For an integrated luminosity of 30 fb^{-1}, the significances with the "best fit" and with the positive/negative deviations are equal respectively to 6.40 and 7.25/5.78 for $M = 1.5$ TeV/c^2, and to 6.83 and 8.54/5.93 for $M = 3.5$ TeV/c^2. The main effect of the variation comes from the gluon-fusion contribution to the graviton production

Table 14.2: The 5 σ discovery limit on the resonance mass (given in TeV/c^2) for the three models, for an integrated luminosity of 10, 30 and 60 fb^{-1}.

Model	Luminosity (fb^{-1})		
	10	30	60
KK Z	4.97	5.53	5.88
G ($c = 0.01$)	1.38	1.64	1.82
G ($c = 0.1$)	3.34	3.81	4.10
Z' (ψ)	2.85	3.31	3.62
Z' (ALRM)	3.76	4.27	4.60

cross section. A lower dependence is observed for the KK Z and Z' channels, which are produced by quark-anti-quark annihilation. For KK Z boson production at $M = 4$ TeV/c^2 with an integrated luminosity of 30 fb^{-1}, the significances with the "best fit" and with the positive/negative errors are equal respectively to 22.5 and 23.3/21.9.

Changing to 1 the value of the K factor of the DY background for RS graviton production increases the significance from 6.39 to 6.87 ($M = 1.5$ TeV/c^2, $c = 0.01$) and from 6.83 to 7.09 ($M = 3.5$ TeV/c^2, $c = 0.1$). The discovery limits increase respectively from 1.64 to 1.68 TeV/c^2 and from 3.81 to 3.84 TeV/c^2.

The data themselves will be used to estimate and cross-check the Drell-Yan background at very high energy. For resonance discovery, the number of events in the side-bands of the resonance and their mass dependence will be used to estimate the number of background events under the resonance peak, provided there is enough data in the side-bands. In this approach, the uncertainties on the background cross-sections, the PDF and the luminosity measurement are highly reduced.

14.2.5 Identification of new particles

Once a resonance is found, information will be gained on its characterisation from the study of other decay channels, like $\gamma\gamma$ (see Section 14.6), of angular distributions and of asymmetries, in view of the spin determination (see also Section 14.3).

As an example, RS gravitons with spin 2 can be distinguished from the Standard Model background and Z' bosons with spin 1 using the distribution of the $\cos\theta^*$ variable, computed as the cosine of the polar angle between the electron and the boost direction of the heavy particle in the latter rest frame. In addition to the cuts defined above, the electron and positron candidates are requested to have opposite charges, in order to identify the electron, from which the $\cos\theta^*$ variable is computed.

The $\cos\theta^*$ distributions for graviton production with M = 1.25 TeV/c^2, $c = 0.01$, and $M =$ 2.5 TeV/c^2, $c = 0.1$, are presented in Fig. 14.5, for an integrated luminosity of 100 fb^{-1}. The error bars represent the corresponding statistical uncertainties, applied to the signal distribution obtained from a large statistics simulation. The spin-2 hypothesis is compared to the spin-1 hypothesis (red curve in the figures), formed by the Drell-Yan production (Figs. 14.5(a) and (b)) or the ALRM Z' production (Figs. 14.5(c) and (d)). For graviton production, the expected background is included in the $\cos\theta^*$ distributions.

The spin 2 nature of RS gravitons can be determined in contrast to the Drell-Yan production or the Z' boson production for an integrated luminosity of 100 fb^{-1} up to 1.25 TeV/c^2 for

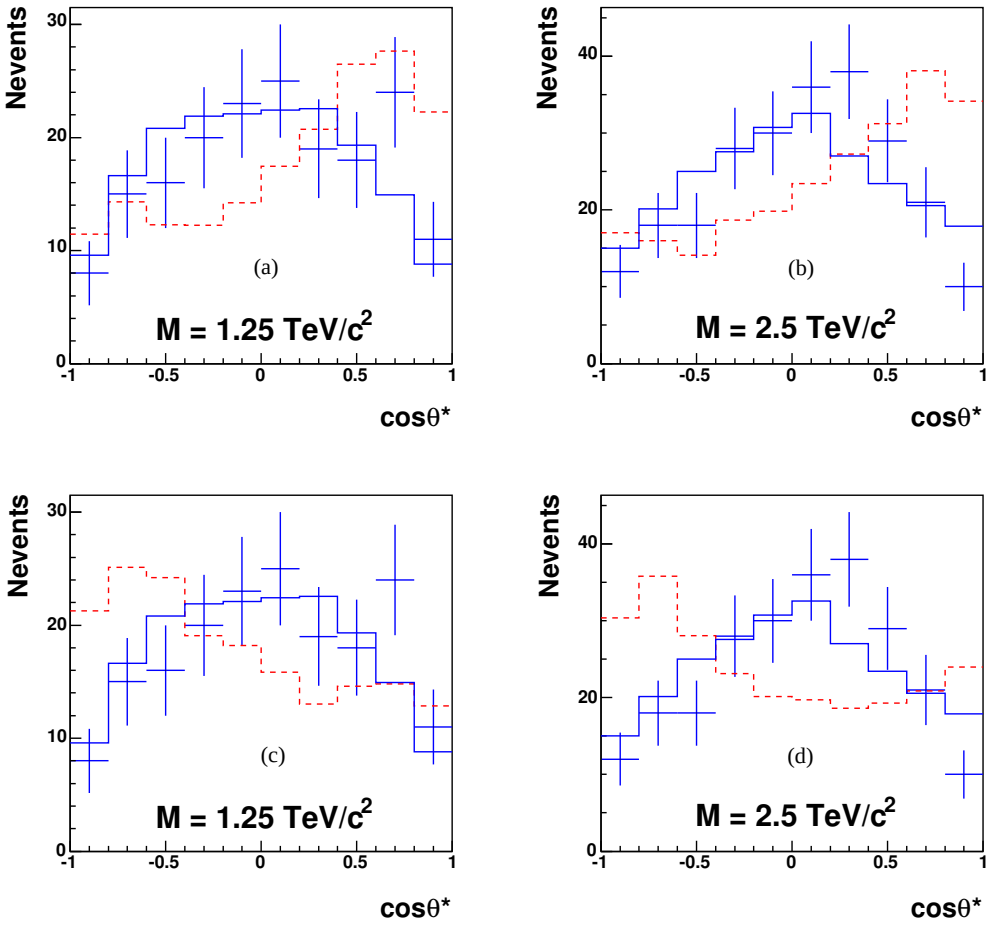

Figure 14.5: Distributions of $\cos\theta^*$ for graviton production (full blue curves) and for Drell-Yan production (dashed red curves) normalised to the signal, for M = 1.25 TeV/c^2 (a) and 2.5 TeV/c^2 (b), and for Z' boson (ALRM model) (red curves), normalised to the signal, for M = 1.25 TeV/c^2 (c) and 2.5 TeV/c^2 (d), with an integrated luminosity of 100 fb^{-1}. The error bars represent the "1-experiment" distribution for the graviton production. The expected background is included in the $\cos\theta^*$ distributions.

$c = 0.01$ and 2.5 TeV/c^2 for $c = 0.1$.

14.3 High mass dimuon final states

Many scenarios beyond the Standard Model are expected to manifest themselves through modifications in the mass spectrum of high-mass dimuon pairs. The potential of the CMS experiment to discover dimuon decays of a new heavy neutral gauge boson, Z′, is discussed in Section 3.3.4; the discovery reach for a representative set of Z′ models was found to be in the range between 2.9 and 3.8 TeV/c^2 for an integrated luminosity of 10 fb^{-1}. In this section, we discuss the observability of $\mu^+\mu^-$ final states predicted in two classes of large extra dimensions models, RS and ADD. While the RS scenario gives rise to relatively narrow resonances, the ADD model is expected to be observed via non-resonant modifications of the

dimuon spectrum; therefore, these two searches require somewhat different experimental approaches. The search for compositeness in the dimuon channel is described in Section 15.2.

Once a new physics is discovered, observables other than dimuon invariant mass can be used to determine the theoretical framework to which it belongs. The measurement of the forward-backward asymmetries of leptonic decay products has long been known as a powerful tool to identify Z′; some aspects of such a measurement at the LHC are discussed in Section 3.3.5. Spin discrimination of new heavy resonances based on an unbinned likelihood ratio statistic incorporating the angles of the decay products is described in Section 3.3.6.

14.3.1 The Randall-Sundrum model in the dimuon channel

We consider the range of RS1 graviton masses in the range $1 < m < 4\,\text{TeV/c}^2$ and the dimensionless coupling constant in the expected theoretical range $0.01 \leq c \leq 0.1$ [721]. A full simulation with PYTHIA [68] version 6.227 and with the GEANT4-based CMS program [8] and reconstruction with the CMS full-reconstruction package [10], including pile-up of minimum-bias collisions is carried out. We derive both the CMS discovery potential for Randall-Sundrum gravitons and the performance of spin determination in this channel (see details in Ref.[116]). The non-reducible backgrounds are the Drell-Yan process, vector boson pair production ZZ, WZ, WW, $t\bar{t}$ production, etc. In the SM the expected leading-order cross section of the Drell-Yan process dominates the other contributions (see the Section 9.2 for details). The trigger simulation is based on the reconstruction package, using the on-line reconstruction algorithm. We require the single or double muon trigger, no requirement for calorimeter isolation of high-p_T muons is made. The total trigger + reconstruction efficiency varies between 95% and 90% for dimuons in the mass range $1 < m < 4\,\text{TeV/c}^2$. Only the events which passed both the Level-1 and HLT cuts are selected. Note that the trigger efficiency is significantly decreased after applying of the calorimeter isolation cuts (down to 15 %). This drop is caused by electromagnetic showers accompanying high-energy muons. In the following, no cuts on calorimeter isolation of muon tracks are applied at the HLT level.

14.3.1.1 The Randall-Sundrum model discovery potential

The significance estimators used for studying the discovery potential of the RS1 model were S_{cP}, S_{cL} and S_L, defined in Appendix A.1 (see discussion of S_L in Section 3.3.4.1).

Figure 14.6a shows the integrated luminosity required for a 5σ discovery as a function of the dimuon mass. The results for different values of integrated luminosity are summarised in Table 14.3 and Figure 14.6b. The CMS experiment can observe a RS1 graviton with mass up to 2.3 TeV/c^2 with an integrated luminosity of $\int L\,dt = 1$ fb^{-1} if the coupling c is equal to 0.1. For $c = 0.01$ the mass reach does not exceed 1.9 TeV/c^2, even for the asymptotic regime of LHC operation with $\int \mathcal{L}\,dt = 300\,\text{fb}^{-1}$. The asymptotic reach limit for $c = 0.1$ is 4.5 TeV/c^2.

A combined analysis [721] in the RS1 scenario shows that the value of the coupling constant c is strongly restricted (Figure 14.6b) due to the theoretical constraints to assure that the model does not introduce a new hierarchy (the scale parameter $\Lambda_\pi = M_{Pl}e^{kL} < 10\,\text{TeV/c}^2$ with the symbols defined in Section 14.1.5). The direct comparison of results on a mass reach region for c with the data of the Figure 14.6 shows that a luminosity of 100 fb^{-1} is needed to test the RS1 model everywhere in ($c - M_{\text{grav}}$) space of model parameters. However, these conclusions are not definitive since the initial theoretical constraints are quite arbitrary.

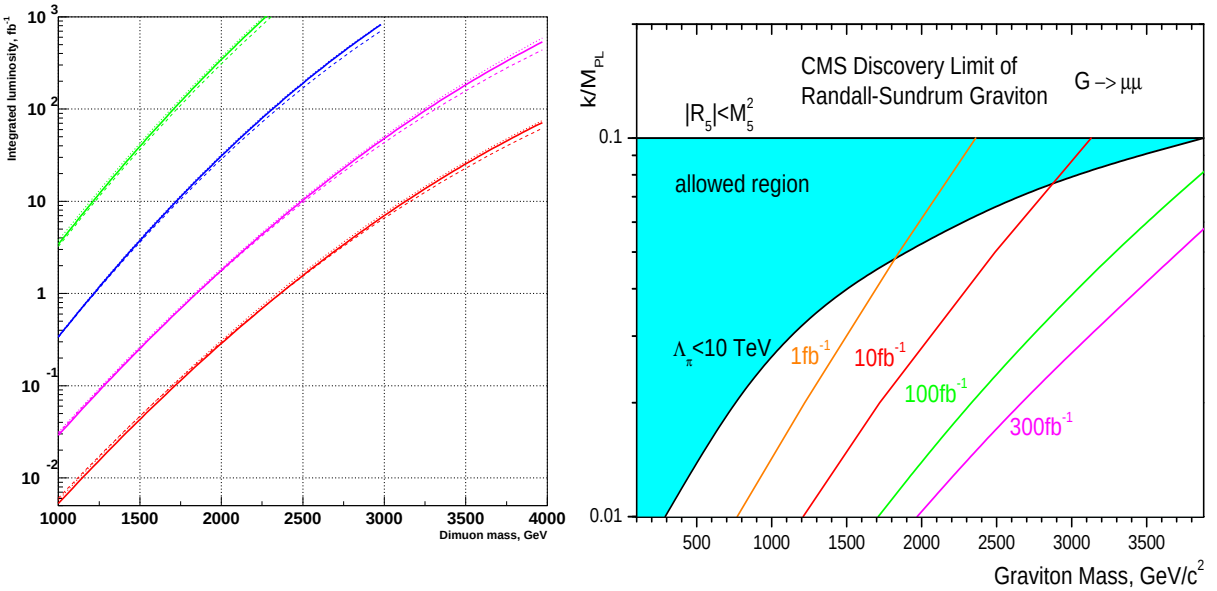

Figure 14.6: Discovery limit for RS1 graviton with $\mu^+\mu^-$ decay mode for different values of RS1 coupling constant $c = 0.01$, 0.02, 0.05 and 0.1 (from top to bottom). Used discovery limit $S > 5$ for the S_{cP} estimator (solid lines), S_L (dashed lines), S_{cL} (dotted lines).
(b) Reach of the CMS experiment as a function of the coupling parameter c and the graviton mass for various values of integrated luminosity. The left part of each curve is the region where significance exceeds 5σ.

14.3.1.2 Systematic uncertainties

The results taking into account the systematic uncertainties are shown in Figure 14.7. The expected effects of misalignment are considered in two misalignment scenarios: the First Data and the Long Term scenarios [98], which correspond to different stages of the alignment corrections for the positions of the tracker and muon chambers. The current estimate is that the transition to the Long Term scenario can be achieved at an integrated luminosity of about $1\,\text{fb}^{-1}$ [85]. In contrast to Figure 14.6 which assumed a K-factor equal to unity, a K-factor of $K = 1.30 \pm 0.05$ is used both for the RS1 signal and Drell-Yan background. Additional variations due to EW corrections, hard-scale and PDF uncertainties have been considered, the details being found in Ref.[116].

14.3.1.3 Spin discrimination in angular analysis

A study of muon angular distributions allows a discrimination between the hypotheses of Graviton (spin-2 particle) and Z' (spin-1 particle) – see the discussion and the results in Sec. 3.3.6.

14.3.2 The ADD model in the dimuon channel

We consider the fundamental Planck scale of the ADD model in the range of $3.0 < M_S < 10.0\,\text{TeV/c}^2$ and numbers of extra dimensions in the range of $3 \leq n \leq 6$ [698]. The contribution of KK-modes of ADD gravitons to the Drell-Yan processes is computed using the leading-order matrix element [722] which was implemented in STAGEN generator collection as external matrix element in PYTHIA [68] version 6.227. A full simulation [8] of the CMS detector and reconstruction [10], without a pile-up of minimum-bias collision is performed to derive the CMS discovery potential for ADD virtual gravitons (see details in Ref.[723]). The

Table 14.3: CMS discovery potential invariant mass reach (in TeV) to observe the RS1 graviton in $\mu^+\mu^-$ channel.

Coupling constant c	Estimator	1 fb^{-1}	10 fb^{-1}	100 fb^{-1}	300 fb^{-1}
0.01	S_{cP}	0.75	1.20	1.69	1.95
	S_{cL}	0.77	1.21	1.71	1.97
	S_L	0.78	1.23	1.73	1.99
0.02	S_{cP}	1.21	1.72	2.30	2.63
	S_{cL}	1.22	1.72	2.31	2.64
	S_L	1.22	1.74	2.34	2.68
0.05	S_{cP}	1.83	2.48	3.24	3.67
	S_{cL}	1.85	2.49	3.26	3.71
	S_L	1.85	2.51	3.31	3.79
0.1	S_{cP}	2.34	3.11	4.12	4.52
	S_{cL}	2.36	3.13	4.14	4.54
	S_L	2.36	3.16	4.23	4.73

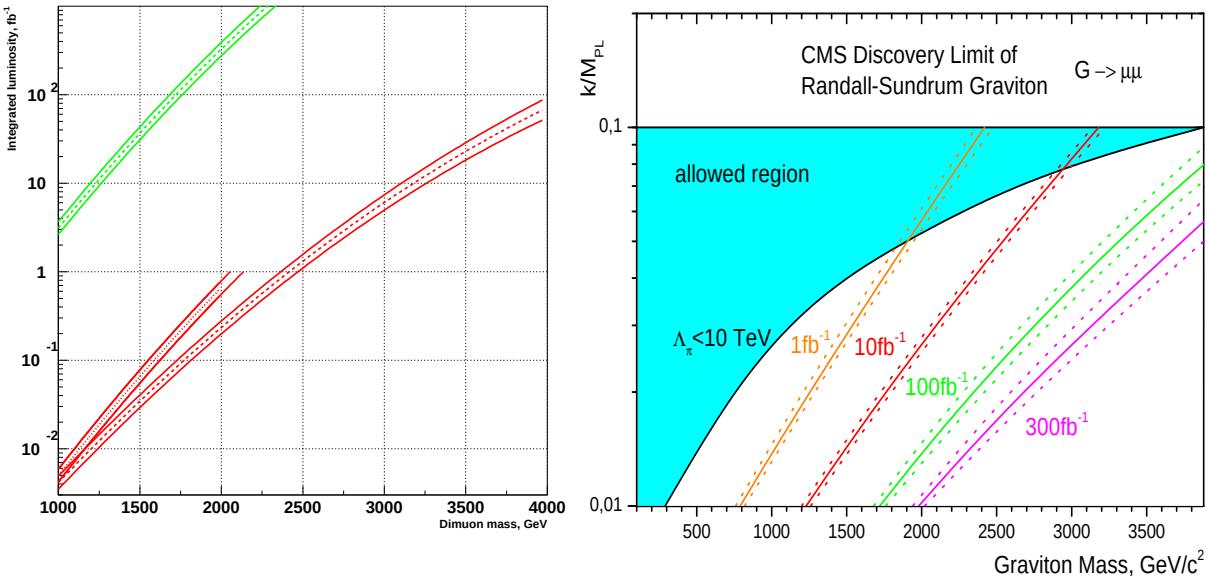

Figure 14.7: (a) Discovery limit for coupling constants $c = 0.01, 0.1$ (upper and lower curves, respectively) after taking into account the systematic uncertainties including misalignment in two scenarios: the curves ending at integrated luminosity of 1 fb^{-1} correspond the First Data misalignment scenario, the other ones correspond to the Long Term scenario. The ranges show the expected variations due to the systematic uncertainties.
(b) The ranges of the expected variations due to the systematic uncertainties for the mass reach of the CMS experiment.

non-reducible backgrounds are the Drell-Yan process, vector boson pair production ZZ, WZ, WW, $t\bar{t}$ production, etc. In the SM the expected leading-order cross section of the Drell-Yan process dominates the other contributions (see the Section 9.2 for details). The trigger simulation is realised in the reconstruction package, using the on-line reconstruction algorithm. A single or double muon trigger is required, but no requirement for calorimeter isolation of high-p_T muons is made. The total trigger + reconstruction efficiency varies between 70% and 90% for dimuons dependent on the model parameters. Only the events which passed both

the Level-1 and HLT cuts are selected.

14.3.2.1 The ADD discovery limit

The CMS discovery potential was estimated using as significance S_{cP} and S_{cL}, defined in Appendix A.1.

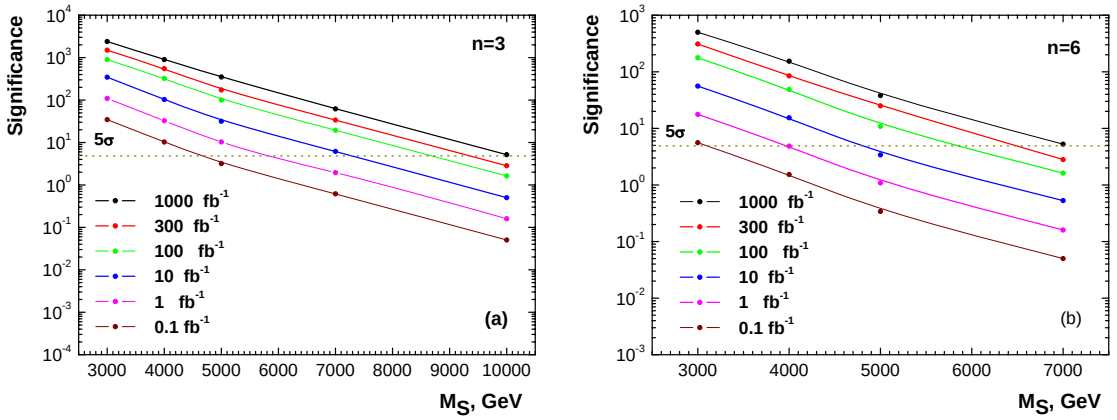

Figure 14.8: Significance as a function of M_S for (a) $n = 3$ and (b) $n = 6$.

The computed significance values for the ideal detector as a function of a fundamental theory scale, M_S, are presented in Fig. 14.8 for integrated luminosities of 0.1, 1.0, 10, 100, 300, 1000 fb^{-1}. The main observations are:

- $\int \mathcal{L}dt = 1\,\text{fb}^{-1}$, even a low luminosity regime allows to measure the effect from the virtual contributions of ADD gravitons to Drell-Yan process for an effective fundamental Planck scale up to 4.0 TeV for the most unfavourable case with $n = 6$. For a scenario where the number of extra dimensions is $n = 3$ the reach limit is extended to 5.8 TeV.
- $\int \mathcal{L}dt = 10\,\text{fb}^{-1}$, M_S values of 4.8 and 7.2 TeV can be reached for $n = 3$ and $n = 6$ respectively.
- $\int \mathcal{L}dt = 100\,\text{fb}^{-1}$, for LHC operation in a high luminosity regime allow the observation of the ADD signal at $5.8 \div 8.7$ TeV of model scale dependent on a number of extra dimensions.
- $\int \mathcal{L}dt = 300\,\text{fb}^{-1}$, in the asymptotic regime the CMS sensitivity to fundamental Planck scale is increased to values of $6.5 \div 9.3$ TeV.

14.3.2.2 Systematics

The results taking into account the systematical uncertainties with the S_{cP} estimator are shown in Figure 14.9. To take into account the misalignment effect two scenario of misalignment were considered during reconstruction procedure: *First Data* scenario [98] for 0.1 and 1.0 fb^{-1} and *Long Term* scenario [98] for 10, 100 300, 1000 fb^{-1}. The K-factor of $K = 1.30 \pm 0.05$ is used both for ADD signal and Drell-Yan background. Additional variations due to hard-scale and PDF uncertainties as well as trigger and selection uncertainties have been considered, the details being given in Ref.[723].

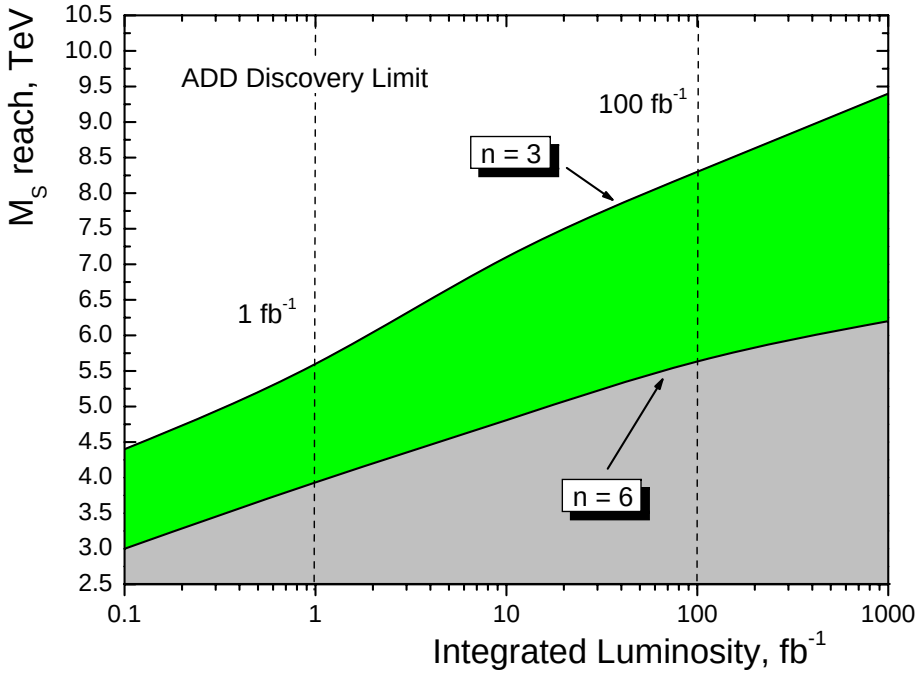

Figure 14.9: 5σ limit on M_S for the number of extra dimensions $n = 3$ and 6.

14.4 High energy single lepton final states

14.4.1 Introduction

Several theoretical models predict, in addition to the well known electroweak vector bosons γ, W, Z, further heavy gauge bosons. These additional particles are postulated for example in Left-Right Symmetric Models [724–727], based on the gauge group $SU(3)_C \times SU(2)_L \times SU(2)_R \times U(1)_{B\text{-}L}$ (B,L: baryon-, lepton-number) in theories predicting a substructure of the known "elementary particles", and in Little Higgs Models [90].

Here we investigate the detection capabilities for a hypothetical heavy partner of the W, a charged spin-1 boson W'. We do not assume one of the specific models mentioned above, but derive the W' properties from the Reference Model by Altarelli [697], which has been used in several earlier experiments, so that the resulting limits can be compared easily. In this Reference Model the W' is a carbon copy of the W, with the very same left-handed fermionic couplings (including CKM matrix elements), while there is no interaction with the Standard Model gauge bosons or with other heavy gauge bosons as a Z'. Thus the W' decay modes and corresponding branching fractions are similar to those for the W, with the notable exception of the $\mathrm{t\bar{b}}$ channel, which opens for W' masses beyond 180 GeV.
In hadron collisions W' bosons can be created through $\mathrm{q\bar{q}}$ annihilation, in analogy to W production. Previous searches for the Reference W' at LEP and at the Tevatron give rise to lower bounds approaching 1 TeV [728].
This analysis is based on the decay $W' \to \mu\nu$, with a branching ratio of roughly 10%. The resulting signature of a high energy muon accompanied by missing energy allows an easy separation of signal and background reactions. More details are found in [729].

14.4.2 Data samples

For this study we assume an integrated luminosity of 10 fb^{-1} and an average instantaneous luminosity of $\mathcal{L} = 2 \times 10^{33}\,\text{cm}^{-2}\,\text{s}^{-1}$ corresponding to an average pile-up of 3.5 pp-collisions per bunch crossing.

Reference Model W' events decaying into muon and neutrino have been generated with PYTHIA v6.227 [68], based on the leading order cross section and the parton density functions CTEQ 5L (leading order) [719]. In total about 300 000 events have been produced for W' masses between 1 TeV and 8 TeV. The product of LO cross section and branching fraction varies between $3.0 \cdot 10^3$ fb (1 TeV) and $3.3 \cdot 10^{-4}$ fb (8 TeV), to be compared with $1.7 \cdot 10^7$ fb for Standard Model W production and muonic decay. The detector response was simulated with the full CMS simulation [8] and reconstruction [10] software. Both the signal events and the following background samples were analysed: $W \rightarrow \mu\nu$, $Z \rightarrow \mu\mu$, WW inclusive, ZZ inclusive, ZW inclusive, $t\bar{t}$ inclusive. These data sets have been produced in the CMS Data Challenge 2004. On average 3.5 minimum bias reactions have been overlaid to each event.

14.4.3 Event selection and analysis

Events have been preselected requiring at least one globally reconstructed muon which pass the trigger criteria.
The final cuts to select $W' \rightarrow \mu\nu$ candidate events are:

- muon quality: at least 13 hits along the global track, $\chi^2/N_{dof} < 50$ for the fit.
- single muon requirement
- muon isolation: no additional track ($p_T > 0.8\,\text{GeV}$) within a cone of size $\Delta R = 0.17$.

These cuts have been chosen to maximise the signal/background ratio.

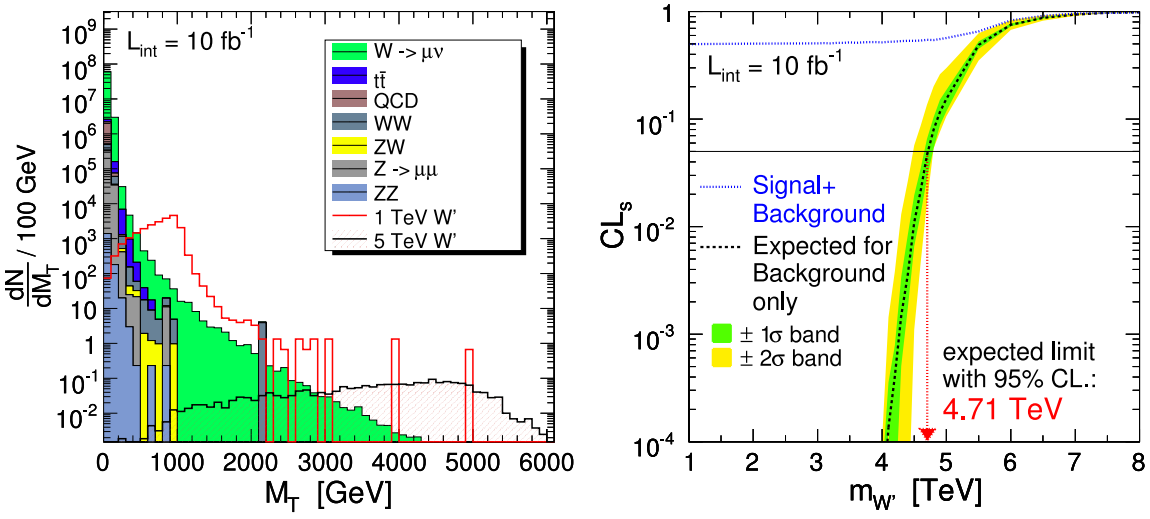

Figure 14.10: **Left:** transverse invariant mass spectrum of signal (1 and 5 TeV, non-stacked) and background (stacked) after applying the selection cuts. **Right:** result of the CL_s-method: with an integrated luminosity of 10 fb^{-1} Reference W' bosons can be excluded up to a mass of 4.7 TeV.

For the selected events the transverse mass

$$M_{\mathrm{T}} = \sqrt{2 p_{\mathrm{T}_\mu} E_{\mathrm{T}}^{\mathrm{miss}} (1 - \cos \Delta\phi_{\mu, E_{\mathrm{T}}^{\mathrm{miss}}})}$$

is calculated from the muon transverse momentum p_{T_μ}, the missing energy component in the transverse plane $E_{\mathrm{T}}^{\mathrm{miss}}$ and the angular $\Delta\phi_{\mu, E_{\mathrm{T}}^{\mathrm{miss}}}$ between both in this plane. Fig. 14.10 shows the resulting distribution for signal (1 and 5 TeV) and background events. The W' boson distributions show a Jacobian peak which is spread out for large M_{T} due to the detector resolution. It can be seen immediately, that a 1 TeV boson can be discovered or excluded easily, while for higher masses a statistical analysis is needed to quantify the sensitivity.

14.4.4 Discovery and exclusion potential

To interpret the results, the $\mathrm{CL_s}$ method [508] is applied, which is based on the likelihood ratios, calculated for all bins of the M_{T} distribution. $\mathrm{CL_s}$ is defined as ratio of the confidence levels for the signal and background hypotheses, $\mathrm{CL_s} = \mathrm{CL_{s+b}}/\mathrm{CL_b}$.
Figure 14.10 shows, that for an integrated luminosity of 10 fb^{-1}, a limit of 4.7 TeV at the 95% CL is reachable, if no signal is present in the CMS data. Both the expected discovery and exclusion limits are displayed in figure 14.11 as a function of integrated luminosity and W'

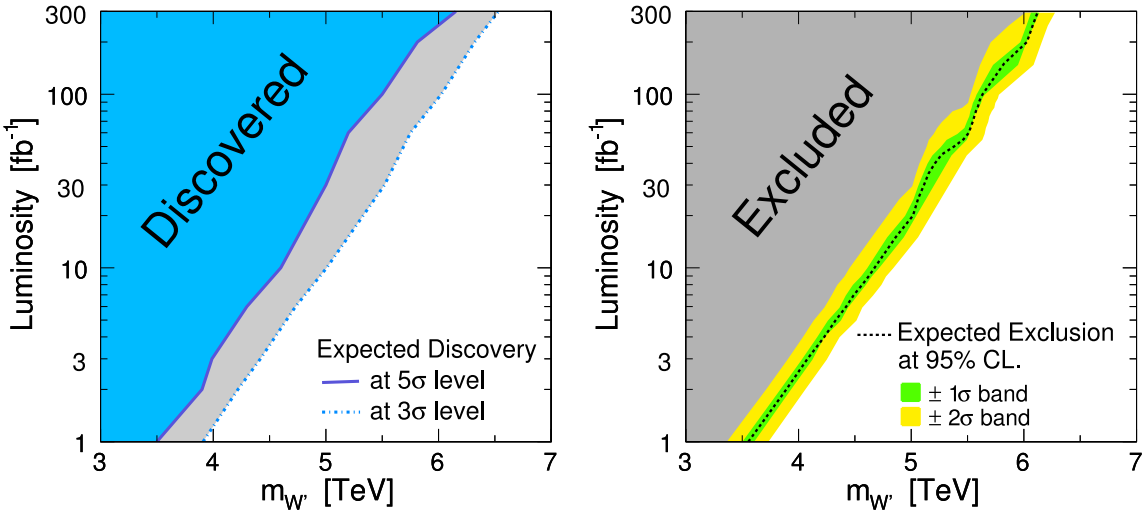

Figure 14.11: The plots show which integrated luminosity is needed to discover (left) or exclude (right) W' bosons of a certain mass.

mass. To investigate the sensitivity to the signal and background cross sections, they have been varied in a wide range; relative changes by factors of 2 and 10, respectively, lead to a lowering of the accessible mass range by about 0.5 TeV in the worst case.

14.4.5 Systematic uncertainties

The uncertainties arising from an imperfect knowledge of the PDFs at LHC energies and the error from the hard scale parameters have been investigated by using the Les Houches Accord PDFs [94] and varying the hard scale, respectively. The relative errors on the cross-section of the signal are listed in Table 14.4. The error on the background is comparable to that of the W' at the corresponding invariant mass.

Table 14.4: Relative systematic uncertainties in percent, arising from an imperfect theoretical knowledge (parton density functions, hard scale) and the expected luminosity error for an integrated luminosity of 10 fb^{-1}.

Systematic Uncertainties					
Type	1 TeV W'	2 TeV W'	3 TeV W'	4 TeV W'	5 TeV W'
PDF $\Delta\sigma/\sigma$	$^{+3.6}_{-4.3}$	$^{+6.8}_{-5.9}$	$^{+6.2}_{-8.3}$	$^{+17.1}_{-10.6}$	$^{+33.7}_{-18.9}$
Hard Scale $\Delta\sigma/\sigma$	$^{+4.1}_{-4.1}$	$^{+7.5}_{-6.9}$	$^{+10.4}_{-9.2}$	$^{+13.1}_{-10.3}$	$^{+14.8}_{-12.7}$
Luminosity $\Delta\mathcal{L}/\mathcal{L}$	$\pm5\%$	$\pm5\%$	$\pm5\%$	$\pm5\%$	$\pm5\%$

The steep falling invariant mass distribution especially of the W background holds a potential danger for the detection of W' bosons: if only a small fraction of these events is reconstructed with a by far too large mass, which might result from a mis-measured muon momentum, the detection of a W' becomes extremely difficult. Such a behaviour would be visible in non-gaussian tails for example in the p_{T} resolution distribution. Using a large sample of a W events it could be demonstrated, that the alignment precision expected after an integrated luminosity of 10 fb^{-1} has only a small influence on the non-gaussian tails of the muon p_{T} resolution distribution.

The luminosity uncertainty at the considered integrated luminosity of 10 fb^{-1} is expected to be 5%, while other experimental errors (neutron background, dead detector components, etc.) are expected to be negligible.

14.4.6 Summary

For an integrated luminosity of 10 fb^{-1}, W' bosons of the Reference Model can be discovered or excluded up to a mass of 4.5–5 TeV, from an analysis of the muonic decay mode.

14.5 High mass dijet final states

14.5.1 Dijet resonances and contact interactions

Dijet resonances and contact interactions are the two major signals of new physics with dijets. Dijet resonances are direct and compelling observations of a new physical object at a mass M, requiring an incoming parton-parton collision energy equal to the mass. Contact interactions (discussed in section 15.3) are indirect observations of an energy scale of new physics, Λ, which can be significantly larger than the available collision energy. Resonances are clear signals but contact interactions are often observed first.

14.5.2 Dijet resonance search

We search for processes producing narrow resonances, X, decaying to dijets: $pp \rightarrow X \rightarrow$ jet + jet (inclusive) [730]. Our experimental motivation is that LHC is a parton-parton collider, and resonances made from partons must decay to the same partons giving two jets in the final state. The theoretical motivation is broad, since there are many models that predict narrow dijet resonances.

14.5.2.1 Dijet resonance models

In Figure 14.12 we show the cross section times branching ratio times acceptance calculated

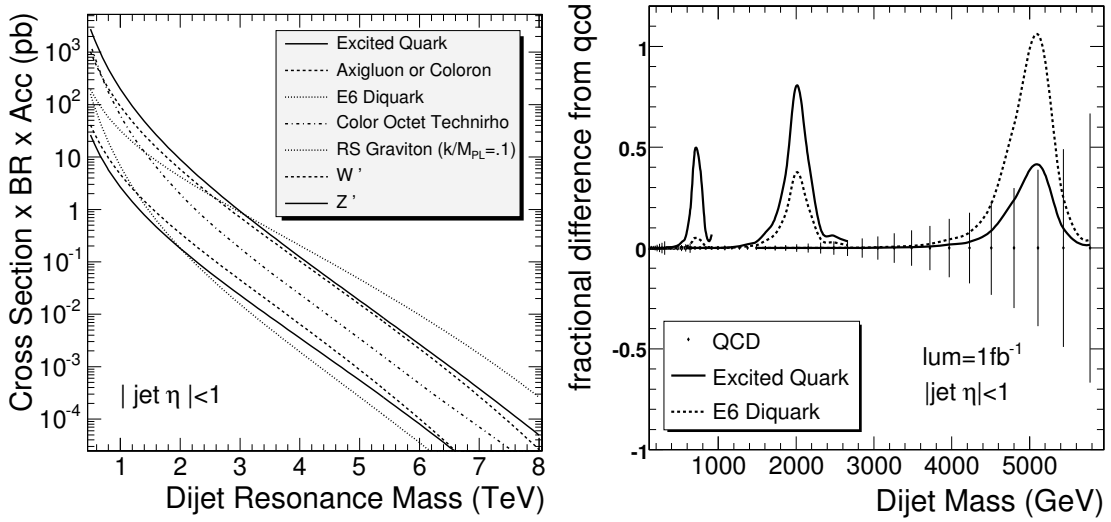

Figure 14.12: (left) The total cross section times branching ratio times acceptance for dijet resonances from eight different models (see text). (right) For resonance masses of 0.7, 2.0, and 5.0 TeV/c^2, the fractional difference between an excited quark (solid curve) or an E6 diquark (dashed curve) and the QCD dijet background is compared to the QCD statistical errors (vertical lines).

to lowest order for eight benchmark models. Here we introduce them in order of descending cross section at low mass. Excited states of composite quarks [731] are strongly produced giving large cross sections ($qg \rightarrow q^*$). Axigluons (A) [732] or colorons (C) [733] from an additional colour interaction are also strongly produced, but require an anti-quark in the initial state ($q\bar{q} \rightarrow A$ or C) slightly reducing the cross section compared to excited quarks. Diquarks [734] from superstring inspired E_6 grand unified models are produced with electromagnetic coupling from the valence quarks of the proton ($ud \rightarrow D$). The cross section for E_6 diquarks at high mass is the largest of all the models considered, because at high parton momentum the probability of finding a quark in the proton is significantly larger than the probability of finding a gluon or anti-quark. Colour octet technirhos [735] from topcolour-assisted technicolour are produced for either gluons or quark-anti-quark pairs in the initial state through a vector-dominance model of mixing between the gluon and the technirho ($q\bar{q}, gg \rightarrow g \rightarrow \rho_{T8}$). Randall-Sundrum gravitons [93] from a model of large extra dimensions are produced with a significant cross section at masses below 1 TeV/c^2 primarily from gluons in the initial state ($q\bar{q}, gg \rightarrow G$). Heavy W bosons [736] inspired by left-right symmetric grand unified models have electroweak couplings and require anti-quarks for their production($q_1\bar{q}_2 \rightarrow W'$) giving small cross sections. Heavy Z bosons [736] inspired by grand-unified models are widely anticipated by theorists, but they are weakly produced, and require an anti-quark in the initial state($q\bar{q} \rightarrow Z'$), so their production cross section is around the lowest of the models considered. Lower limits from CDF [119] and D0 [120] on the mass of these models range from 0.4 to 1.0 TeV/c^2.

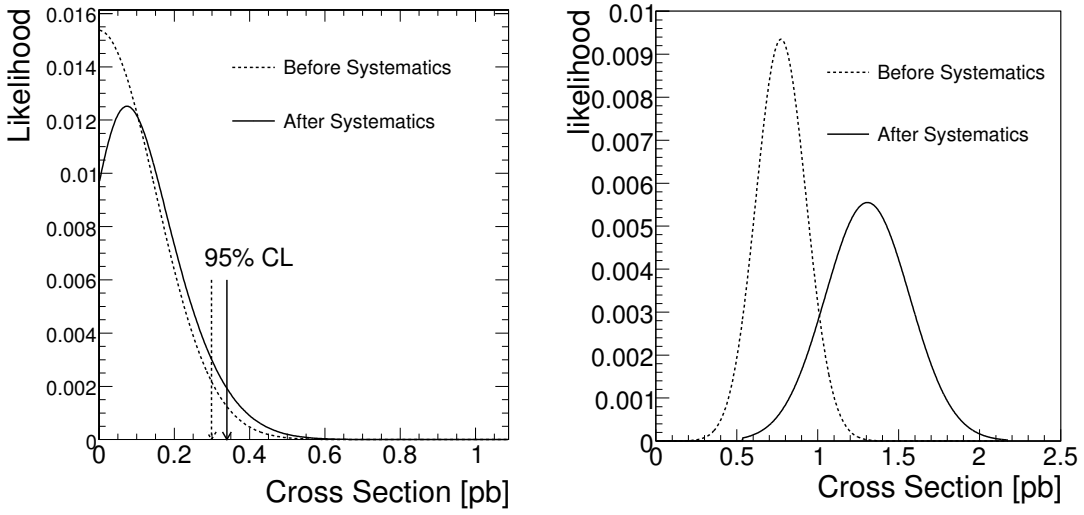

Figure 14.13: Likelihoods for observing a narrow dijet resonance of mass 2 TeV/c^2 in a 1 fb^{-1} data sample that contains only QCD background (left) and a data sample that also contains a resonance with a significance of 5σ (right) are shown with statistical uncertainties only (dashed) and including systematics (solid).

14.5.2.2 Dijet resonance sensitivity estimates

The signal and background dijet mass distributions for narrow resonances were presented in section 4.1.4. In Figure 14.12 we demonstrate the size of the signal for excited quarks and E_6 diquarks compared to the QCD background and it's statistical uncertainty. It is clear that we will be sensitive to such large signals for strongly produced dijet resonances. Here we quantify our sensitivity to any model of narrow dijet resonances. In Figure 14.13 we show examples of likelihoods for excluding or observing a narrow resonance signal on a QCD background as a function of the signal cross section. In the case where the observed sample is QCD only, the signal likelihood peaks around zero cross section, and the 95% CL excluded signal cross section is shown. In the case where the observed sample is QCD plus a resonance signal, we have varied the signal size until the Gaussian distributed likelihood is 5 σ above zero. In figure 14.13 we have included estimates of our systematic uncertainties. For a resonance mass of 0.7 (5.0) TeV/c^2 the systematic uncertainty on the observable signal cross section due to the jet energy uncertainty in the background rate is 15% (25%), the uncertainty due to jet resolution in the resonance shape is 10% (10%), the uncertainty due to radiation's affect on the resonance shape is 10% (25%), and the uncertainty due to luminosity is 10% (10%). For resonance masses just above the dijet mass thresholds where the trigger prescale decreases, there is an additional systematic uncertainty from the jet energy uncertainty. Systematic uncertainties have a greater effect on discovery than exclusion, because exclusions occur at a smaller signal cross section and are dominated by statistical uncertainties.

Figure 14.14 demonstrates that the 95% CL exclusion and 5σ discovery signal cross sections, including statistical uncertainties only, have reasonable values when compared to the size of the QCD statistical errors. Also in Figure 14.14 we present the resonance cross section values for jet $|\eta| < 1$ that CMS can expect to exclude at 95% CL or discover at 5σ significance for an integrated luminosity of 1 fb^{-1}. These can be compared with the cross section of any model of narrow dijet resonances, and here we compare with our benchmark models.

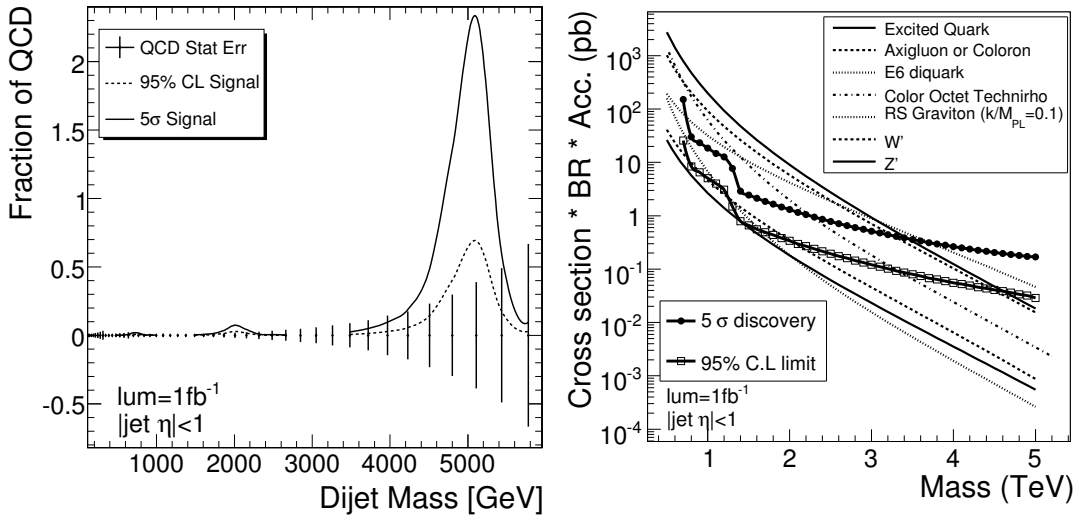

Figure 14.14: Left) For resonances of mass 0.7, 2.0 and 5.0 TeV/c^2, the rate as a fraction of QCD that CMS expects to exclude (dashed) or discover (solid) including statistical uncertainties only. Right) The resonance cross section that CMS expects to exclude (boxes) or discover (circles), including systematic uncertainties, is compared to the cross section for eight resonance models.

From Figure 14.14 we can read off the mass limits or discoveries that are possible with 1 fb^{-1} of data, which are listed in Table 14.5 along with the results of repeating the same analysis for 100 pb^{-1} and 10 fb^{-1}. The resonances that are produced via the colour interaction (excited quarks, axigluons, colorons and colour octet technirhos) or from the valence quarks of each proton (E_6 diquarks) have large cross sections and can be discovered up to a mass of a few TeV. A single search for resonances in the dijet mass distribution provides CMS with a sensitive test of many different models of the widely anticipated new physics at the TeV scale.

14.6 High mass diphoton final states

14.6.1 Introduction

The study of the Randall-Sundrum(RS) graviton decaying into the two photons is particularly interesting as the detection of such few TeV/c^2 mass resonance in such channel together with its observation in the dilepton channel will sign a RS graviton, distinguishing it from a Z′ production. The model is governed by two parameters: the graviton mass M and its coupling to Standard Model particles c, the latter being related to the natural width of the resonance.

14.6.2 Event generation and kinematics pre-selection

The search for the G $\rightarrow \gamma\gamma$ signal at LHC is affected by four types of backgrounds:

- The prompt diphoton production from the quark annihilation and gluon fusion diagrams, which provides an intrinsic or 'irreducible' background.
- The γ + jets production consisting of two parts: i) prompt photon from hard in-

Table 14.5: Sensitivity to dijet resonances with $100\,\text{pb}^{-1}$, $1\,\text{fb}^{-1}$, and $10\,\text{fb}^{-1}$. For each resonance model, we show the range of masses we expect to be able to exclude at a confidence level of 95% or greater, and the range of masses we expect to be able to discover with a significance of 5σ or greater. All estimates are with both statistical and systematic uncertainties.

Resonance Model	95% CL Excluded Mass (TeV/c^2)			5σ Discovered Mass (TeV/c^2)		
	$100\,\text{pb}^{-1}$	$1\,\text{fb}^{-1}$	$10\,\text{fb}^{-1}$	$100\,\text{pb}^{-1}$	$1\,\text{fb}^{-1}$	$10\,\text{fb}^{-1}$
Excited Quark	0.7 - 3.6	0.7 - 4.6	0.7 - 5.4	0.7 - 2.5	0.7 - 3.4	0.7 - 4.4
Axigluon or Colouron	0.7 - 3.5	0.7 - 4.5	0.7 - 5.3	0.7 - 2.2	0.7 - 3.3	0.7 - 4.3
E_6 diquarks	0.7 - 4.0	0.7 - 5.4	0.7 - 6.1	0.8 - 2.0	0.8 - 3.7	0.8 - 5.1
Colour Octet Technirho	0.7 - 2.4	0.7 - 3.3	0.7 - 4.3	0.7 - 1.5	0.7 - 2.2	0.7 - 3.1
Randall-Sundrum Graviton	0.7 - 1.1	0.7 - 1.1 1.3 - 1.6	0.7 - 1.1 1.3 - 1.6 2.1 - 2.3	N/A	N/A	N/A
W′	0.8 - 0.9	0.8 - 0.9 1.3 - 2.0	0.8 - 1.0 1.3 - 3.2	N/A	N/A	N/A
Z′	N/A	N/A	2.1 - 2.5	N/A	N/A	N/A

teraction + the second photon coming from the outgoing quark due to final state radiation and ii) prompt photon from hard interaction + the decay of a neutral hadron (mostly isolated π^0) in a jet, which could fake a real photon.

- The background from QCD hadronic jets, where electromagnetic energy deposits result from the decay of neutral hadrons (especially isolated π^0s) in both jets.
- Drell Yan process with $e + e-$ in a final state which could mimic photons when correspondent electron tracks will not be assigned to the superclusters during the reconstruction.

Generator-level pre-selection and parameters used for QCD and bremsstrahlung backgrounds is described in [737].

14.6.3 Offline selection and analysis

The requirements for the analysis were as follows:

1 Two super-clusters (SCs) with $E_{\text{T}} > 150\,\text{GeV}$ and two HLT trigger bits triggered at the same time: 2p (two photons) and r2p (two photons relaxed).

2 Calorimeter isolation criteria: for each SC the energy in a cone of $\Delta R = 0.5$ (excluding SC itself) should be $< 0.02 E_{\text{T}}(SC)$

3 $E(HCAL)/E(ECAL) < 0.05$

4 Tracker isolation: the sum of the energy of all tracks in a cone $\Delta R = 0.5$ around the SC should be $< 0.01 E_{\text{T}}(SC)$

5 Photon energy corrections are done in a simple way so far:

- For E1 energy $< 1.7\,\text{TeV}$, only a simple energy dependent part of correction is applied (just a shift of the peak)
- For E1 energy $> 1.7\,\text{TeV}$, the MGPA saturation correction (1d) was applied (see and [738])

14.6.4 K-factors

To produce the final results and to calculate the expected statistical significance for RS-1 graviton search recently calculated next-to-leading order corrections (K factors) to the cross sections of different types of background are used: K = 1.5 for quark annihilation [26], K = 1.2 for gluon fusion [29], K = 1 for the γ + hadronic jets [29] and K = 1 for QCD jets. For signal, a conservative K= 1 value is taken.

14.6.5 Results

The numbers of events passing the analysis cuts described above, for the signal and for the backgrounds, are presented in Table 14.6 (1.5 TeV/c^2, 0.01) and in Table 14.7 (3.5 TeV/c^2, 0.1).

Table 14.6: Number of events passed through the analysis cuts defined above for $M_G = 1.5$ TeV/c^2, $c = 0.01$ and $\mathcal{L} = 30\,\text{fb}^{-1}$. Leading column is non-saturated events, all saturated events, passed through the analysis, were added in brackets, where applied.

	signal	Born (k=1.5)	Box (k=1.2)	Brem (k=1)	QCD (k=1)	DY (k=1)
trigger + 2SC	28.9	8.6	0.10	29.2	798.7	4.3
+ EM isolation	24.5	5.5	0.08	20.3	361.8	3.5
+ HCAL/ECAL	24.3	5.4	0.08	4.4	12.8	3.5
+ tracker isolation	17.6	4.2(+0.2)	0.05	0.17	0.0	0.0

Table 14.7: Number of events passed through the analysis cuts defined above for $M_G = 3.5$ TeV/c^2, $c = 0.1$ and $lumi = 30\,\text{fb}^{-1}$. Leading column is non-saturated events, all saturated events, passed through the analysis, were added in brackets, where applied.

	signal	Born (k=1.5)	Box (k=1.2)	Brem (k=1)	QCD (k=1)	DY (k=1)
trigger + 2SC	11.6	0.20	$4.4 * 10^{-4}$	0.78	821.9	0.10
+ EM isolation	10.8	0.14	$3.6 * 10^{-4}$	0.32	164.4	0.095
+ HCAL/ECAL	10.6	0.13	$3.4 * 10^{-4}$	0.016	0.0	0.095
+ tracker isolation	8.9(+1.0)	0.10(+0.02)	$2.7(+0.24) * 10^{-4}$	$1.7 * 10^{-3}$	0.0	$7.2 * 10^{-4}$

Figure 14.15 shows the number of events satisfying all cuts for both signal and backgrounds for the cases (1.5 TeV/c^2, 0.01) and (3.0 TeV/c^2, 0.1) after 30 fb^{-1} luminosity. The results for one year low luminosity of 10 fb^{-1} are presented in Figure 14.16.

Taking into account the K-factors described above, the number of events for signal and background and the significance S_{cL} (defined in Appendix A.1) for $c = 0.01$ and $c = 0.1$ are shown respectively in Tables 14.8 and 14.9 for an integrated luminosity of 30 fb^{-1}.

The significance as a function of the graviton mass (M_G) for integrated luminosities of 10 fb^{-1}, 30 fb^{-1} and 60 fb^{-1} are displayed in Figure 14.17.

The discovery region in the plane of the coupling parameter c and the graviton mass is shown in Fig. 14.18.

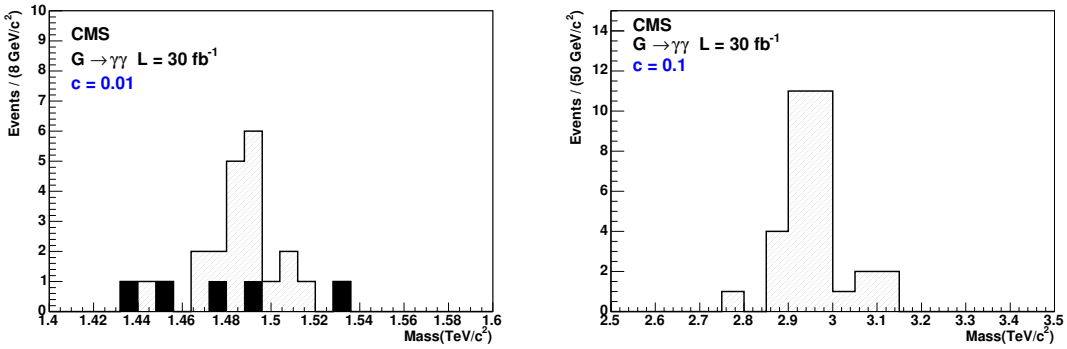

Figure 14.15: Number of events passing all cuts for (1.5 TeV/c^2, 0.01) (left) and (3.0 TeV/c^2,0.1) (right) RS-1 gravitons for 30 fb^{-1} integrated luminosity.

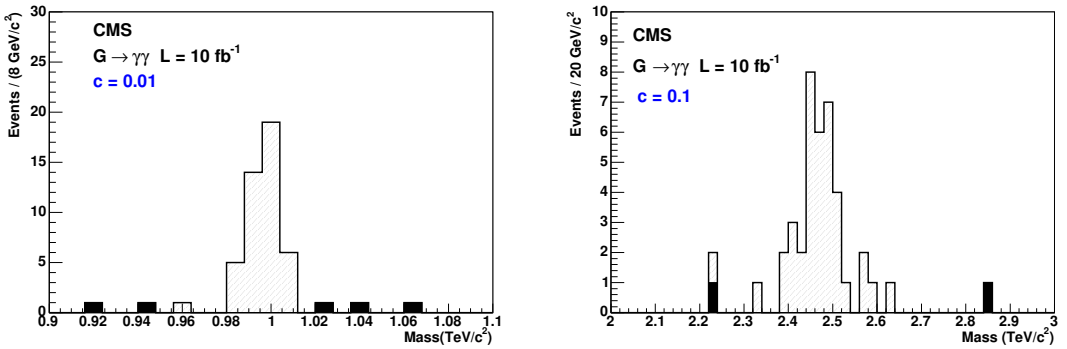

Figure 14.16: Number of events passing all cuts for (1.0 TeV/c^2, 0.01) (left) and (2.5 TeV/c^2,0.1) (right) RS-1 gravitons for 10 fb^{-1} integrated luminosity.

Table 14.8: Significance for $c = 0.01$ and $\mathcal{L} = 30\,\text{fb}^{-1}$

	$M_G = 1.0$ TeV/c^2	$M_G = 1.25$ TeV/c^2	$M_G = 1.5$ TeV/c^2	$M_G = 1.75$ TeV/c^2	$M_G = 2.0$ TeV/c^2
N_s	135.8	44.0	17.6	7.3	3.9
N_{bkg}	15.0	8.8	4.6	1.8	1.2
Significance	20.6	10.1	5.9	3.9	2.6

Table 14.9: Significance for $c = 0.1$ and $\mathcal{L} = 30\,\text{fb}^{-1}$

	$M_G = 2.5$ TeV/c^2	$M_G = 3.0$ TeV/c^2	$M_G = 3.5$ TeV/c^2	$M_G = 4.0$ TeV/c^2	$M_G = 4.5$ TeV/c^2
N_s	103.8	31.6	9.9	3.44	1.11
N_{bkg}	1.11	0.35	0.13	0.06	0.02
Significance	27.3	15.0	8.2	4.6	2.6

The discovery region for 60 fb^{-1} extends to $M_G = 1.82$ TeV/c^2 if $c = 0.01$ and to $M_G = 4.27$ TeV/c^2 if $c = 0.1$. For 30 fb^{-1} it is $M_G = 1.61$ TeV/c^2 if $c = 0.01$ and $M_G = 3.95$ TeV/c^2

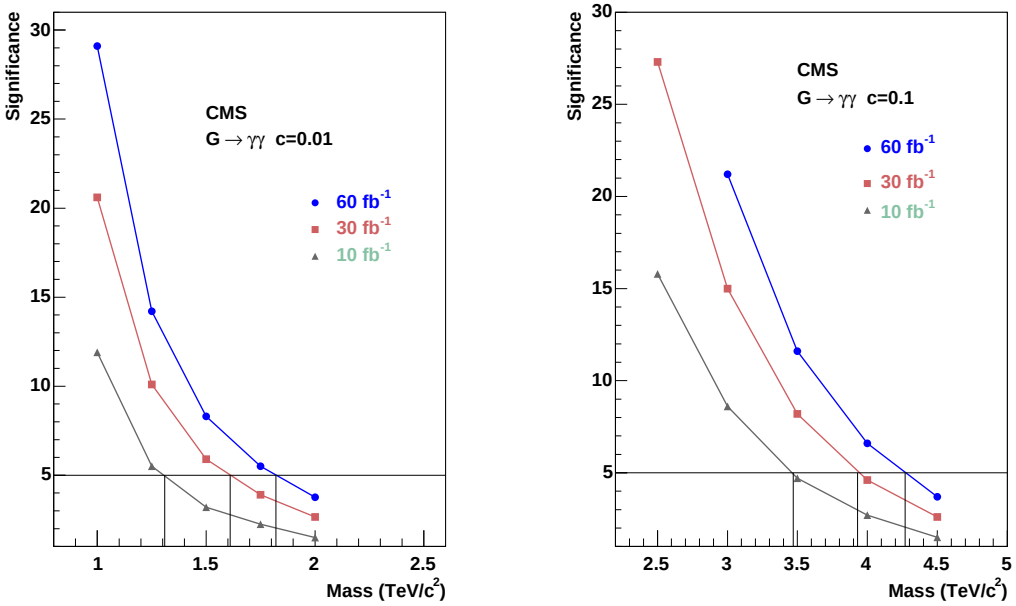

Figure 14.17: Significance as a function of the graviton mass for 10 fb^{-1}, 30 fb^{-1} and 60 fb^{-1} integrated luminosities, with c=0.01 (left) and c=0.1 (right)

if $c = 0.1$. For 10 fb^{-1} it reaches to $M_G = 1.31$ TeV/c^2 if $c = 0.01$ and $M_G = 3.47$ TeV/c^2 if $c = 0.1$.

14.6.6 Systematic uncertainties for 30 fb^{-1}

Several systematic uncertainties and their effect on the mass reach have been evaluated for an integrated luminosity of 30 fb^{-1}. The effect of hard scale uncertainties is given in Table 14.10, computed by multiplying and dividing the scale $\hat{s}$ by a factor 2. The uncertainties

Table 14.10: Hard scale confidence limits uncertainties for 30 fb^{-1}

	$4\hat{s}$	$0.25\hat{s}$
$c = 0.01$	-62 GeV/c^2	+56 GeV/c^2
$c = 0.1$	-47 GeV/c^2	+42 GeV/c^2

from the pdfs, computed with LHApdf, amount for $c = 0.01$ to -55 GeV/c^2 and for $c = 0.1$ to -152 GeV/c^2. There is another source of uncertainties due to the fact, that we have used K-factor = 1.5 for the Born process, while the most recent measurements at the Tevatron pointed to a K-factor closer to 2 [739]. The effect of such a change on the mass reach is -50 GeV/c^2 for $c = 0.01$ and -30 GeV/c^2 for $c = 0.1$.

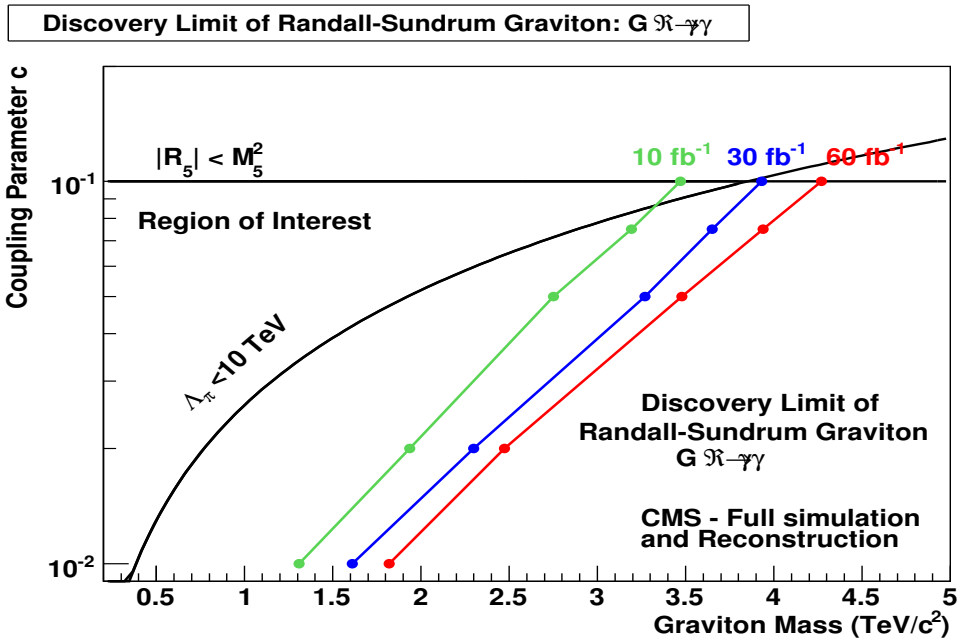

Figure 14.18: Reach of the CMS experiment in the search for the Randall-Sundrum graviton decaying into diphoton channel as a function of the coupling parameter c and the graviton mass for $10\,\mathrm{fb}^{-1}$, $30\,\mathrm{fb}^{-1}$ and $60\,\mathrm{fb}^{-1}$. The left part of each curve is the region where the significance exceeds 5σ.

14.7 Single γ final state with $E_{\mathrm{T}}^{\mathrm{miss}}$ from extra dimensions

14.7.1 Topology of single-photon final states

An introduction to the signals involving direct graviton emission in ADD type of extra dimensions frameworks is given is section 14.3.2. The topology of single photon events can be identified by:

- a single high p_{T} photon in the central η region
- high missing p_{T} back-to-back to the photon in the azimuthal plane with a similar p_{T} distribution.

These characteristics are not strongly dependent on the ADD model parameters. The details of this analysis can be found in [740].

14.7.2 Backgrounds from the Standard Model

All signal and background samples used in the following were simulated using the CMS fast detector simulation [11]. Fully simulated reference samples were generated for the signal and the largest irreducible background, $Z^0\gamma \rightarrow \nu\bar{\nu} + \gamma$. A detailed comparison of the resolution, efficiency and purity of all reconstructed objects used in this analysis to the GEANT-based CMS simulation confirmed that the fast simulation provides a very good approximation of the expected detector response. All samples were consistently generated using a generator level cut in PYTHIA $\hat{p_T} > 400\,\mathrm{GeV}$. The backgrounds considered in the study are, $Z^0\gamma \rightarrow \nu\bar{\nu} + \gamma$, $W^{\pm} \rightarrow \ell\nu$ where ℓ is electron, muon or tau, $W^{\pm}\gamma \rightarrow e\nu$+$\gamma$ γ+Jets, QCD, diγ and Z^0 + jets. For the main background, a normalisation method from measured data

is developed employing the reconstructed leptonic decays of the Z^0 into muon and electron pairs.

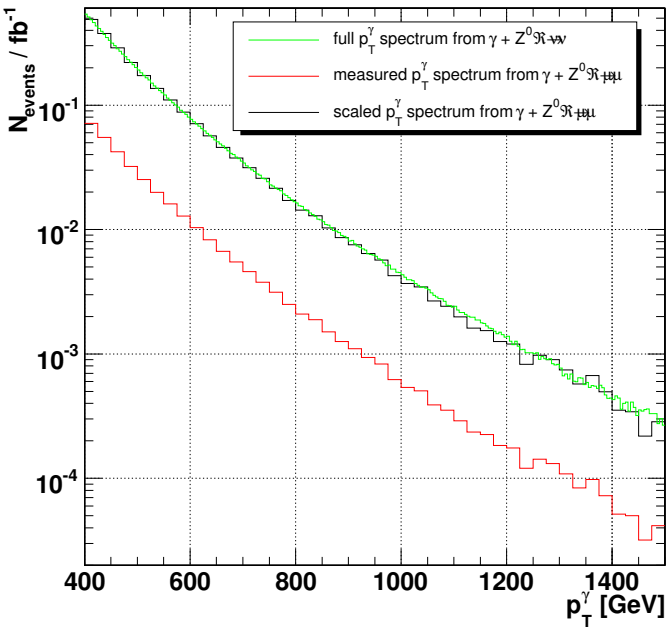

Figure 14.19: Number of expected p_T^γ events per 25 GeV bin at 1 fb^{-1} from measured γ+$Z^0 \to \mu^+\mu^-$ events before and after transformation compared with the generator distribution for γ+$Z^0 \to \nu_i\bar{\nu}_i$ – the transformed muon distribution models the $\nu_i\bar{\nu}_i$ spectrum well.

The detector acceptance for selecting the leptons is parameterised using a two-dimensional function $\alpha(p_T^\gamma, \eta_\gamma)$. Figure 14.19 shows the measured and the p_T^γ spectrum from γ+$Z^0 \to \mu^+\mu^-$ after the (acceptance $\times$ efficiency) parameterisation is applied, in comparison with the generator spectrum for γ+$Z^0 \to \nu_i\bar{\nu}_i$ events. For $p_T^\gamma > 100$ GeV/c there is 1170 $Z^0 \to \mu^+\mu^-/e^+e^-$ events expected after all selection cuts for 30 fb^{-1}. These can be used as the candle sample that provides a direct normalisation of the γ+$Z^0 \to \nu_i\bar{\nu}_i$ with a statistical precision of 3%.

14.7.3 Event selection

The main trigger path for the selection of signal and background events will be the single photon trigger, both at the Level-1 and the HLT. Presently the single photon trigger has a HLT level threshold of 80 GeV, which is far below the selection cut for events with isolated photons above 400 GeV used here. Hence the expected trigger efficiency is close to 100% and its efficiency can be monitored from data with a $E_{\mathrm{T}}^{\mathrm{miss}}$ trigger which will have a threshold in the range of $200 - 300$ GeV, well below the acceptance of the bulk of the signal. Both the topological characteristic and the necessity to reduce the Standard Model background lead to the following selection criteria:

- At least a $E_{\mathrm{T}}^{\mathrm{miss}} > 400$ GeV is required and the photon p_{T} has to be above 400 GeV.
- $|\eta|$ of the photon < 2.4
- $\Delta\phi(E_{\mathrm{T}}^{\mathrm{miss}}, \gamma) > 2.5$
- A track veto for high p_{T} tracks > 40 GeV is applied. This is a powerful criterion to

reduce all backgrounds containing high-energetic charged particles (such as $e^{\pm}$, $\mu^{\pm}$, jets)

- An Isolated Photon Likelihood criterion is applied to remove residual background from hard photon emission from jets as well as fake photons from jets.

Figure 14.20 shows the missing transverse energy spectra for events surviving the selection path for both the signal and the backgrounds. As expected the $Z^0\gamma$ is by far the most dominant component of the background, followed by $W^{\pm}\gamma$ while the contributions of the other Standard Model backgrounds are small. For all ADD cross section the hard truncation approach is used (see section 14.1), i.e. events with $M_G < M_D$ are rejected.

14.7.4 Systematic uncertainties and discovery potential

We consider an uncertainty of 2% for the measurement of the photon p_T^{γ} in the electromagnetic calorimeter and an uncertainty of 5% for the $E_{\mathrm{T}}^{\mathrm{miss}}$ measurement. The resulting decrease of the significance is 1.0% and 1.6% respectively. For the main background the systematics can be reduced to the luminosity measurement using the Z^0 candle calibration method. It can thus be measured with a precision of 3% after $30\,\mathrm{fb}^{-1}$. The $5\,\sigma$ discovery reach is achievable for M_D <2.5 TeV/c^2 and all values of extra dimensions while for M_D <3 TeV/c^2 $5\,\sigma$ reach is achievable for n between 2 and 4. Figure 14.21 shows the expected significances as function of M_{D}.

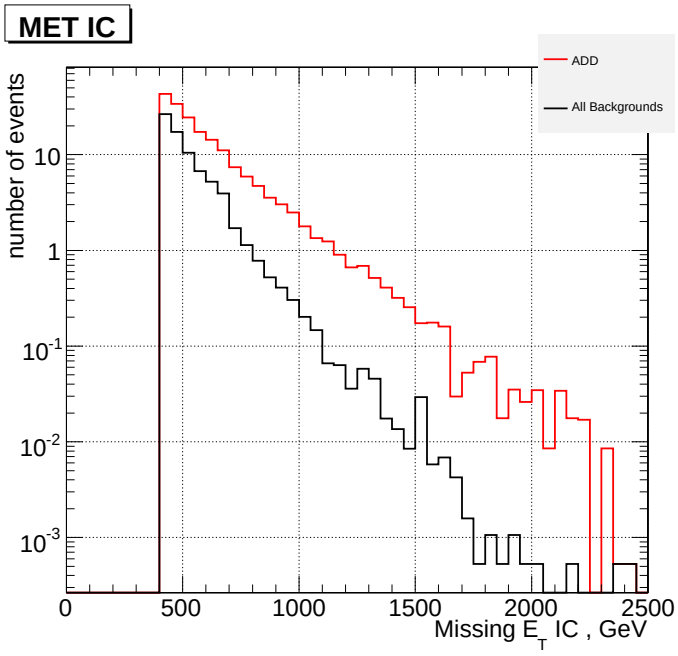

Figure 14.20: Spectrum of the missing E_T for all backgrounds (black histogram) and for an example signal sample ($M_{\mathrm{D}} = 2.5\,\mathrm{TeV}$, $n = 2$). The number of events corresponds to an integrated luminosity of $30\,\mathrm{fb}^{-1}$.

14.8 Black holes

14.8.1 Introduction to higher-dimensional black holes

One of the consequences of large extra dimensions is the possibility to produce microscopic black hole (BH) at LHC energies. Such a BH formed in a (4+n)-dimensional space-time has a Schwarzschild radius

$$r_{s(4+n)} = \frac{1}{\sqrt{\pi} M_{(4+n)}} \left(\frac{M_{BH}}{M_{(4+n)}} \left(\frac{8\Gamma((n+3)/2)}{n+2} \right) \right)^{\frac{1}{n+1}} \tag{14.18}$$

where $M_{(4+n)}$ is the reduced Planck scale and n is the number of large extra dimensions [741]. A high energy collision of two partons can result in the formation of a BH when the impact parameter is smaller than $r_{s(4+n)}$. In the semi-classical approach the BH cross section is given by $\sigma(M_{\mathrm{BH}}) = \pi r^2_{s(4+n)}$ at the parton level. If for low masses $M_{(4+n)}$, *i.e.* around 2 TeV, the BH production cross sections at the LHC is in the pb range.

Once produced, these BHs are expected to decay thermally via Hawking radiation [742]. The Hawking temperature for a BH in 4 + n dimensions is [743]

$$T_{(4+n)} \sim M_{(4+n)} (M_{(4+n)}/M_{\mathrm{BH}})^{1/(n+1)} \tag{14.19}$$

These BHs have a very short lifetime typically of $\sim 10^{-27}$ seconds.

BH events are expected to evaporate democratically by emission of all particle types that exist in nature, independent of their spin, charge, quantum numbers or interaction properties. Therefore they can be a source of new particles. BH physics at the LHC can provide the possibility of probing quantum gravity in the lab.

14.8.2 Analysis selection path and results

Black hole event samples were produced using the CHARYBDIS event generator [744]. As a benchmark the case which is analysed has the following parameters: a) 2 TeV/c^2 effective Planck scale, b) 4 TeV/c^2 minimum and 14 TeV/c^2 maximum black hole mass c) 3 extra dimensions. Time evolution during Hawking radiation and gray body effects are included. The

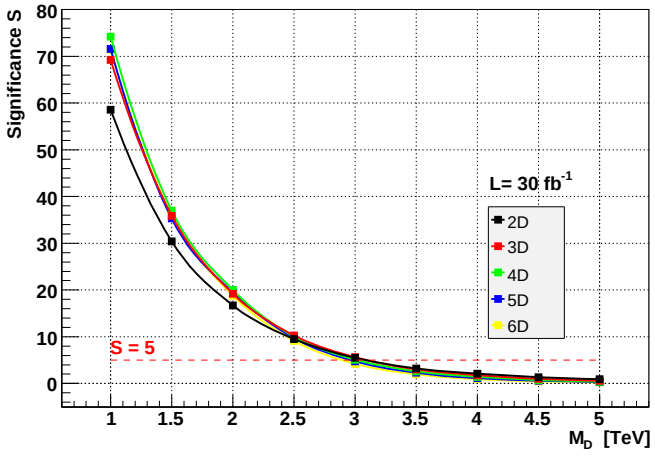

Figure 14.21: Expected significances as function of M_{D} for different number n of extra dimensions.

detector response was simulated by us using the CMS fast simulation (FAMOS, version 1.4.0) after validation against the detailed CMS GEANT-based simulation. The Standard Model backgrounds taken into account include QCD jets, top production and boson plus jet production. The invariant mass of all final state objects (electrons, photons, jets and muons) in the event is found to be correlated with the input black hole mass. In addition since the black hole formation can only occur if $M_{\rm BH} > M_{(4+n)}$, the event invariant mass can indicate the effective Planck scale $M_{(4+n)}$. In the benchmark scenario the invariant mass is required to be greater than 2 TeV/c^2. BH events are characterised by a high multiplicity of the final state particles, which increase as a function of the BH mass (and decreases as a function of Hawking temperature). In particular the ratio of jets to leptons is found to be 5 to 1. In this study with a simple jet and lepton multiplicity counting the jet/lepton ratio is formed. The average value of this ratio is found to be 4.5. The thermal nature of Hawking radiation requires the distribution of BH remnants to be spherical as shown and a sphericity of 0.28 is required which eliminates drastically the Standard Model backgrounds. The invariant mass distribution and sphericity for the signal and background events is shown in figure 14.22.

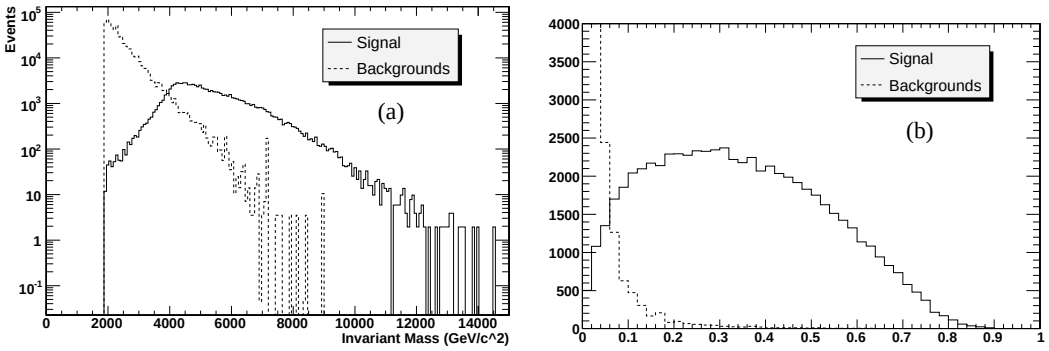

Figure 14.22: (a) Reconstructed invariant mass distribution and (b)event sphericity for black hole and standard model background events

Events are counted when the total sum of the P_T of all reconstructed objects plus the missing transverse energy is larger than 2500 GeV. A study of the Level-1 and HLT trigger path shows that the 4 jet trigger has a 93% efficiency for the signal events and is used in the analysis.

The event selection criteria applied to the reconstructed events and the efficiencies of the requirements are listed in Table 14.11.

Table 14.11: Event selection and background rejection for signal events and major background processes

Cut	Signal	tt+nJ	W+nj	Z+nJ	QCD Dijet	WW+nJ
Cross Section (pb)	18.85	371	896	781.84	33076.8	269.91
Events (10 fb^{-1})	188500	3.71×10^6	8.96×10^6	7.82×10^6	3.31×10^8	2.70×10^6
MInv $>$ 2 TeV/c^2	18.71	13.29	6.53	3.85	2634.94	20.53
Tot. Multiplicity >4	17.72	13.25	6.43	3.84	2613.18	20.42
Sphericity >0.28	9.27	1.60	0.23	0.10	53.74	0.07
Final No.Events (10 fb-1)	92740	15990	2328	982	537391	740

The minimum integrated luminosity needed for 5σ significance and for the benchmark point is $\sim$2 pb^{-1}. A survey of the parameter space using 25 points shows that for effective Planck

scale of 2-3 TeV, minimum black hole mass up to 4 TeV and 2-6 extra dimensions the 5 sigma significance can be obtained with luminosity between fraction of pb^{-1} and 100's of pb^{-1}. For effective Planck scale of 4 TeV a few fb^{-1} is needed for discovery. To account for the systematic uncertainties in the number of signal events, the effect of PDF distribution on cross section is calculated using the CTEQ6 NLO PDF set with the help of LHAPDF interface. PDF uncertainties for the chosen benchmark point is found to be $^{+24.2\%}_{-9.07\%}$. Using these uncertainties, the error in significance calculation was computed to be %12.

14.9 Discussion

The results on Z′s and RS gravitons in the channels studied in this chapter are summarised here.

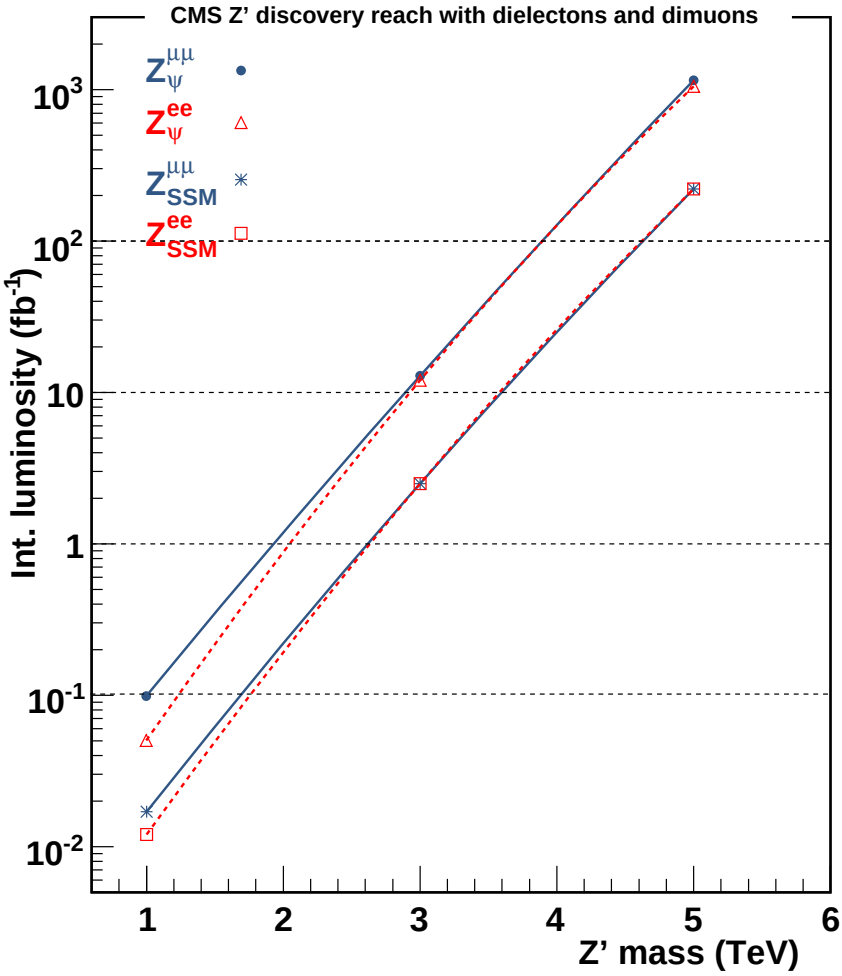

Figure 14.23: Z′ discovery reach for two of the models studied in the dielectron and dimuon channels. The reach for the rest of the models studied is within the band between the two shown here.

In Figure 14.23 the summary of the discovery reach in the dielectron and dimuon channels is shown for two representative Z' models. The reach for the rest of the models studied lies

within the band of the two shown in the figure. The results for the dielectron channel are using here K-factor of 1.3 for the signal and background in order to be directly compared with the dimuon results. Although the analysis strategies and significance computation is different between the two analyses the results are compatible. For low luminosity and mass reach up to 3 TeV/c^2 the muons suffer from misalignment effects which are recovered after 10 fb^{-1}. For high mass reach (above 3 TeV/c^2) the saturation in the ECAL is causing a degradation of the resolution in the dielectron channel. The reach using the dielectron channel is up to 3 TeV better that the dimuons due to less than 1% resolution. Optimising the analysis in the dielectron channel to extract the background from the data and detailed studies of the saturation is expected to further improve the reach in the dielectron channel for high masses. The combined reach of the two channels requires a detailed analysis and is not presented here. Note that a 1 TeV/c^2 Z′ is observable with less than 0.1 fb^{-1} for all models and with a single channel while every TeV/c^2 in mass reach corresponds to approximately an order of magnitude increase in integrated luminosity.

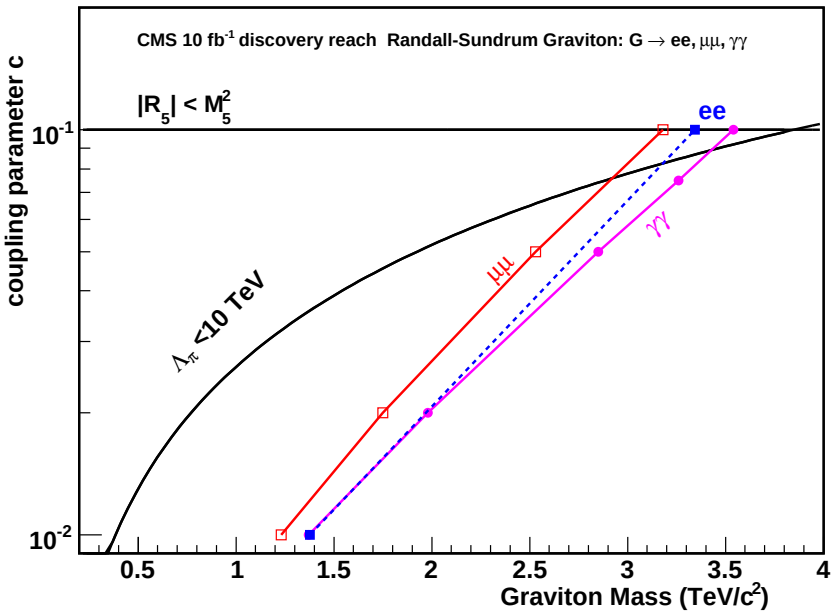

Figure 14.24: RS graviton discovery mass reach as a function of the model coupling parameter in the dielectron, dimuon and diphoton channels for 10 fb^{-1}. The dielectron reach is shown as dashed because only the boundary points (c=0.01 and c=0.1) where studied.

In Figure 14.24 the summary of the RS graviton discovery reach in the dielectron, dimuon and diphoton channels is shown. Here the results for the diphoton channel are using CTEQ6M PDFs to be directly compared with the dielectron and dimuon channels [†] Although the branching ratio to photons is roughly twice that of electrons or muons the reach for low coupling and graviton mass is comparable between dielectrons and diphotons due to the QCD and prompt photon backgrounds in the photon channel which are harder to efficiently

[†]In the main analysis the diphoton channel uses CTEQ5L while the dielectron and dimuon analyses use CTEQ6M where the gluon-gluon contribution is enhanced compared to the CTEQ5L; While the Drell-Yan background is largely insensitive to this choice, at low masses the gluon-gluon is the dominant graviton production process while at high masses the qq dominates where CTEQ5L and CTEQ6M are comparable.

suppress. For higher masses and coupling the diphoton is leading the reach due to the higher branching ratio. The dimuon channel is trailing the reach compared to the dielectrons merely due to resolution.